CONSUMERS BIG ROCK POINT

NUCLEAR POWER REACTOR STABILITY ANALYSIS

By

J. M. Case
L. K. Holland

Prepared for
The U. S. Atomic Energy Commission

under
Contract AT(04-3)-361

ATOMIC POWER EQUIPMENT DEPARTMENT
GENERAL ELECTRIC COMPANY
SAN JOSE, CALIFORNIA

Approved By: S. Levy /cj.
S. Levy
Project Engineer

D H Imhoff
D. H. Imhoff, Manager
Engineering Development

TABLE OF CONTENTS

LIST OF ILLUSTRATIONS

SUMMARY

The analytical model conceived for this stability analysis includes analytical representations of reactor kinetics, fuel rod dynamic heat transfer, hydrodynamic flow characteristics including two-phase effects, and thermodynamic effects due to load and subcooling changes. The hydrodynamic portion of the analytical model is the distinguishing feature of this stability analysis. It is based upon the physical concepts of momentum interchange, conservation of energy, and continuity of mass. These analytical representations are derived from the basic defining differential equations of physical phenomena and are, in turn, transformed into transfer functions. The stability investigation was accomplished by performing a frequency-phase shift analysis (Bode analysis) on the analytical model. The power conditions at which stability was investigated were 50%, 100% and 125% rated power for the 50 MWe core and 100% rated power for the 75 MWe core. In addition, the 50 MWe core was analyzed for the probable operating flux noise level at the 100% power condition.

The results of the Big Rock stability analysis are summarized below, instability being indicated by zero phase and gain margin.

Reactor Condition	Phase Margin	Gain Margin
50 MWe core at 50% rated power	66°	15 db
50 MWe core at 100% rated power	68°	14 db
50 MWe core at 125% rated power	87°	11 db
75 MWe core at 100% rated power	28°	6 db

The 50 MWe core is seen to be stable at all power levels investigated. The stability margins of the 75 MWe core, although somewhat less than those of the 50 MWe core, conservatively indicate that no serious stability problems will be encountered in this mode of operation.

The results of the noise performance analysis for the 50 MWe core at 100% rated power, based on an arbitrary disturbance in inlet subcooling, are given below:

Core Condition	Maximum Predicted Noise Level
Unorificed fuel elements in the center of the core	7.45% peak to peak
Fuel elements in the center of the core with 5 psi inlet orificing	1.35% peak to peak

Fuel element inlet orificing has a significant damping effect upon parallel flow channel mechanisms which in turn, increase the attenuation of reactor flux noise. If the center fuel elements of the Big Rock core are not orificed for the initial startup and the resulting flux noise is objectionable, a remedy is indicated -- raise the single-phase orifice pressure drop over the entire core.

All of the results obtained in this study were obtained by assuming that the rate of change of reactivity due to 100% change in voids for the given power operating condition is $4.50. This is conservatively high for all cases considered, and in particular for partial rated power conditions.

INTRODUCTION

This report presents the results of an analysis which was undertaken to investigate the power stability of the Consumers Big Rock Point Nuclear Power Reactor. The 50 MWe plant was studied for stability at three different power levels; 50% rated, 100% rated and 125% overpower. In addition the 50 MWe core was analyzed for the probable operating flux noise level at the 100% power condition. The 75 MWe plant was studied for stability at the 100% rated power condition only. All of the above points at which stability was investigated were analyzed on the basis of the latest plant design information available at the time of the analysis.

The analytical model conceived for this study to evaluate the hydrodynamic and nuclear stability characteristics of the Big Rock core and nuclear steam supply system is an extension of the nuclear thermal hydraulic feedback network which was used to describe the plant performance of the T-7 natural circulation reactor.[1] The model incorporated an analytical representation of reactor kinetics, fuel rod dynamic heat transfer, hydrodynamic flow characteristics, including two-phase effects, and thermodynamic effects due to load and subcooling changes.

The hydraulic portion of this feedback network is the distinguishing feature of the analytical model. It has its origin in the principles which were developed for the steady state digital computer code HERCULES.[2] These principles have since been broadened to include the transient behavior of natural circulation vertical two-phase flow[3] and the resulting analytical flow model has produced predictions which correspond well with experimental data.[4] It should be noted that, prior to the initiation of this study, the transient analytical flow model was confined to only natural circulation problems. During the course of this investigation, the analytical model was modified and the digital computer code was correspondingly adapted to facilitate the hydrodynamic analysis of the Big Rock forced circulation nuclear steam supply system.

It is believed that the stability limits of high power density boiling water reactors will be determined, in large measure, by the flow behavior of the two-phase nuclear steam supply system. For this reason particular emphasis was placed on developing what is considered to be an accurate and comprehensive analysis of forced circulation two-phase flow dynamics.

THE ANALYTICAL MODEL

The analytical model which was used to analyze the hydrodynamic and nuclear stability characteristics of the Consumers core and nuclear steam supply system is presented in block diagram form in Figure 1. The logic of the model consists of analytical representations of physical phenomena. These representations, or transfer functions, are transformed from basic defining differential equations and describe the linearized phase and magnitude relationships between two variables (output and input) as a function of frequency. The various transfer functions employed in the analytical model are shown diagramatically in Figure 1 as boxes in the flow logic paths. The following are descriptions of the analytical representations used in the stability model.

Reactor Kinetics

The reactor kinetics transfer function is a single delay group - linear representation of the thermal fission (neutron density - N* in per unit values) of slightly enriched U-235 as a result of excess reactivity (ΔK). This relationship was derived from a linearized form of the conventional six delay groups kinetics simulation.(5)

$$\frac{N^*}{\Delta K} = \frac{1}{S\left[\frac{\ell^*}{B} + \sum_{i=1}^{6} \frac{B_i/B}{S + 1/\tau_i}\right]} \qquad (1)$$

Collapsing the six delay groups into a single average time constant and rearranging:

$$\frac{N^*}{\Delta K} = \frac{B}{S\left[\ell^* + \frac{B\bar{\tau}}{\bar{\tau}S+1}\right]} \qquad (2)$$

recognizing that ℓ^* is very small compared with the product of $B\bar{\tau}$:

$$\frac{N^*}{\Delta K^*} = \frac{\frac{1}{\bar{\tau}}(1+\bar{\tau}S)}{S\left[1+\left(\frac{\ell^*}{B}\right)S\right]} \qquad (3)$$

The properties of the delayed neutrons were taken from Design Engineering Data(6) and are presented in Table I.

FIGURE I
CONSUMERS BIG ROCK STABILITY ANALYSIS
BLOCK DIAGRAM

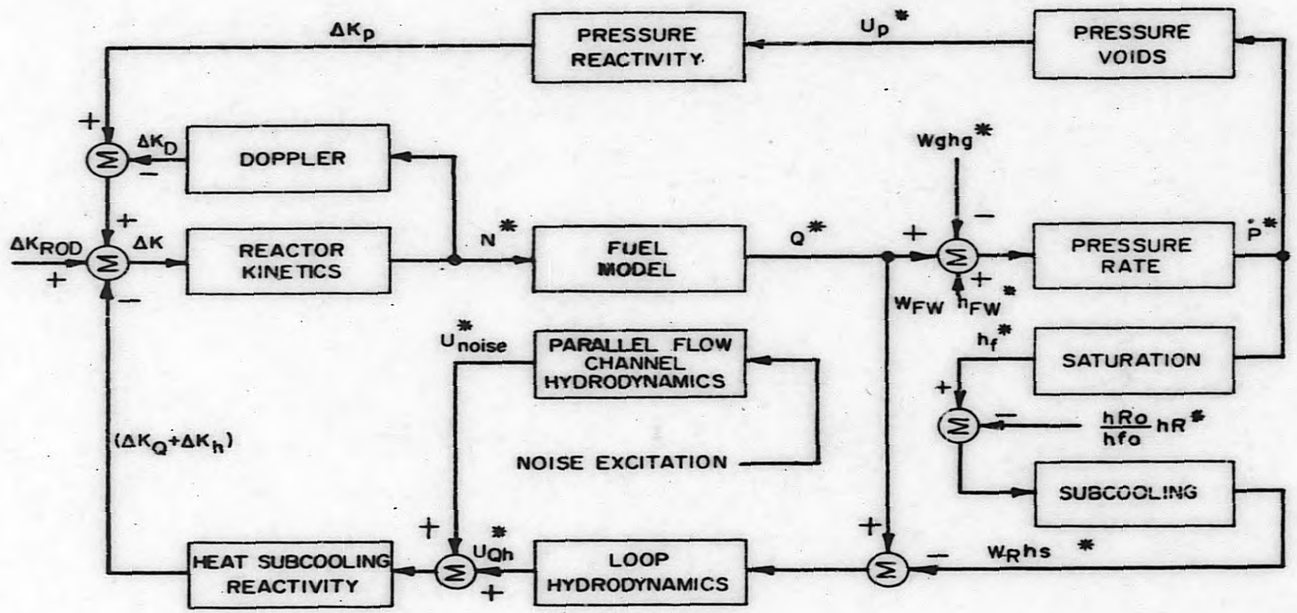

TABLE I

Delay Group	Mean Life ti (sec.)	Decay Constant 1/ti (sec.-1)	Fraction Bi/B
1	80.39	0.0124	0.033
2	32.78	0.0306	0.219
3	8.97	0.112	0.196
4	3.32	0.302	0.395
5	0.880	1.14	0.115
6	0.332	3.02	0.042

$B = 0.0065 \pm 0.0002$

$\ell^* = 5 \times 10^{-5}$ sec.

Solving for the average mean life ($\bar{t}$) from Table I and substituting the appropriate values into Equation (3):

$$\frac{N^*}{\Delta K} = \frac{0.077[1+13(S)]}{S[1+0.0078(S)]} \qquad (4)$$

Fuel Model and Doppler Model

The fuel model is a linear transformation of the thermal diffusion equation which relates the heat imparted to the fluid at the surface of the fuel element (Q* in per unit values) to the neutron density (N*). The Doppler model is a linear representation of the regenerative effect on excess reactivity (ΔK) owing to a change in average fuel temperature, which in this model is related to neutron density (N*). These relationships are based upon a transient analysis of the temperature and heat transfer characteristics of a cylindrical rod with internal heat generation.[7] This analysis has been incorporated into a digital computer code (FTC) which provides transient expressions for surface heat flux, average fuel rod temperature, and center fuel rod temperature as functions of neutron power level.

The following transfer functions were obtained for the Big Rock fuel elements by the use of the digital computer solution:

$$\frac{Q^*}{N^*} = \frac{[1+0.1(S)][1+2.74(S)]}{[1+8.64(S)][1+(S)]} \quad (FUEL) \qquad (5)$$

$$\frac{\overline{T}^{*(AVERAGE)}}{N^*} = \left[\frac{1+2.17(S)}{[1+8.64(S)][1+1.63(S)]}\right] \qquad (6)$$

From Reference [6] the Doppler coefficient of reactivity was found to be $-0.726\ \overline{T}$ (AVERAGE):

$$\frac{\Delta K_D^*}{N^*} = -.726\left[\frac{1+2.17(S)}{[1+8.64(S)][1+1.63(S)]}\right] \quad (DOPPLER) \qquad (7)$$

The Hydrodynamic Analysis

The hydrodynamic portion of the analytical model is the distinguishing feature of this stability analysis. It is based upon the physical concepts of momentum interchange, conservation of energy, and continuity of mass and not upon steam void versus quality correlations, or assumed ratios or differences between steam velocity and water velocity in the two-phase region. This hydrodynamic analysis is defined by a system of six transient equations which describe the mechanics and thermodynamics of two-phase flow loops. The independent variables of the hydrodynamic model include: heat input to the fluid and subcooling of the single-phase inlet fluid to the heater, the dependent variables include: single-phase inlet fluid velocity, two-phase pressure drop, steam velocity in the two-phase flow region, water velocity in the two-phase flow region, average steam volume fraction in the two-phase section and steam volume fraction at boiling boundary of the heater. The only dependent variable needed for this stability analysis, however, was the boiling boundary steam volume fraction $U^*_{Q,h}$ (see Figure 1). A detailed description of the hydrodynamic model is presented in Appendix A. The associated code development is also discussed therein.

The model was applied to the stability analysis in two different ways:

A. Loop hydrodynamics - the reactor core, two-phase risers, steam drum, and recirculation loop was investigated for its feedback contribution to system stability, and

B. Parallel flow channel hydrodynamics - a single hot channel within the reactor core was investigated for its performance in parallel with the rest of the core for flux noise predictions. Individual channels within the reactor core operating in a parallel flow channel arrangement can be appreciably more underdamped than the whole or lumped core and still not adversely affect reactor

stability. They will, however, contribute significantly to the operating flux noise by permitting disturbances in the radial and axial flux distribution to be perpetuated.

The transfer functions applicable to A and B, above, are of the same form. From Appendix A:

$$\frac{U^*_{Q,h}}{Q^*} = \frac{(\text{GAIN 1})[1+\tau_1(S)][1+\tau_2(S)]}{[1+2\xi_1\tau_3(S)+\tau_3^2(S)^2][1+\tau_4(S)]} \qquad (8)$$

$$\frac{U^*_{NOISE}}{EXCITATION} = \frac{(\text{GAIN 2})[1+\tau_5(S)][1+\tau_6(S)]}{[1+2\xi\tau_7(S)+\tau_7^2(S)^2][1+\tau_8(S)]} \qquad (9)$$

The numerical values of gains 1 and 2 and τ_1 through τ_8 in the above two equations must be determined for each operating condition of the reactor. This restriction arises from the fact that the transfer functions as they appear in Equations 8 and 9 are linearized simplifications of a non-linear model. Therefore, they are considered in this stability investigation to be only valid for small variations.

Pressure Rate

The pressure rate transfer function is a linear relationship which describes the time rate of pressure change in the nuclear steam supply system ($\dot{P}^*$) with respect to the energy balance of steam flow rate and enthalpy ($W_g h_g^*$) reactor heat (Q^*) and feedwater flow rate and enthalpy ($W_{FW} h_{FW}^*$). This relationship is based upon mass, volume, and energy balance equations written for the reactor vessel, two-phase riser, steam drum and recirculation loop (see Figure 2). The process assumed for this model is: On a pressure drop, the steam and all of the saturated water remain saturated, and enthalpy and specific volume follow the saturation lines. On a pressure rise the steam and that part of the saturated water that is mixed with the steam remain saturated, and enthalpy and specific volume follow the saturation line. The remaining saturated water is subcooled by the pressure rise and does not change enthalpy. A detailed description of this model has been presented in an earlier report.[8]

$$\dot{P} = \frac{Q - W_{FW}(h_f - h_{FW}) + \frac{h_{fg}}{v_{fg}}(W_{FW} - W_g) - h_{fg} W_g}{\left[W_g \frac{\Delta h_g}{\Delta P} + W_f \frac{\Delta h_g}{\Delta P} - \frac{V}{J}\right] - \frac{h_{fg}}{v_{fg}}\left[W_g \frac{\Delta v_g}{\Delta P} + W_f \frac{\Delta v_f}{\Delta P}\right]} \qquad (10)$$

Assuming the denominator (D_1) remains constant, which is a close approximation, that $W_{FW} \approx W_g$ and omitting external disturbances not considered, and simplifying:

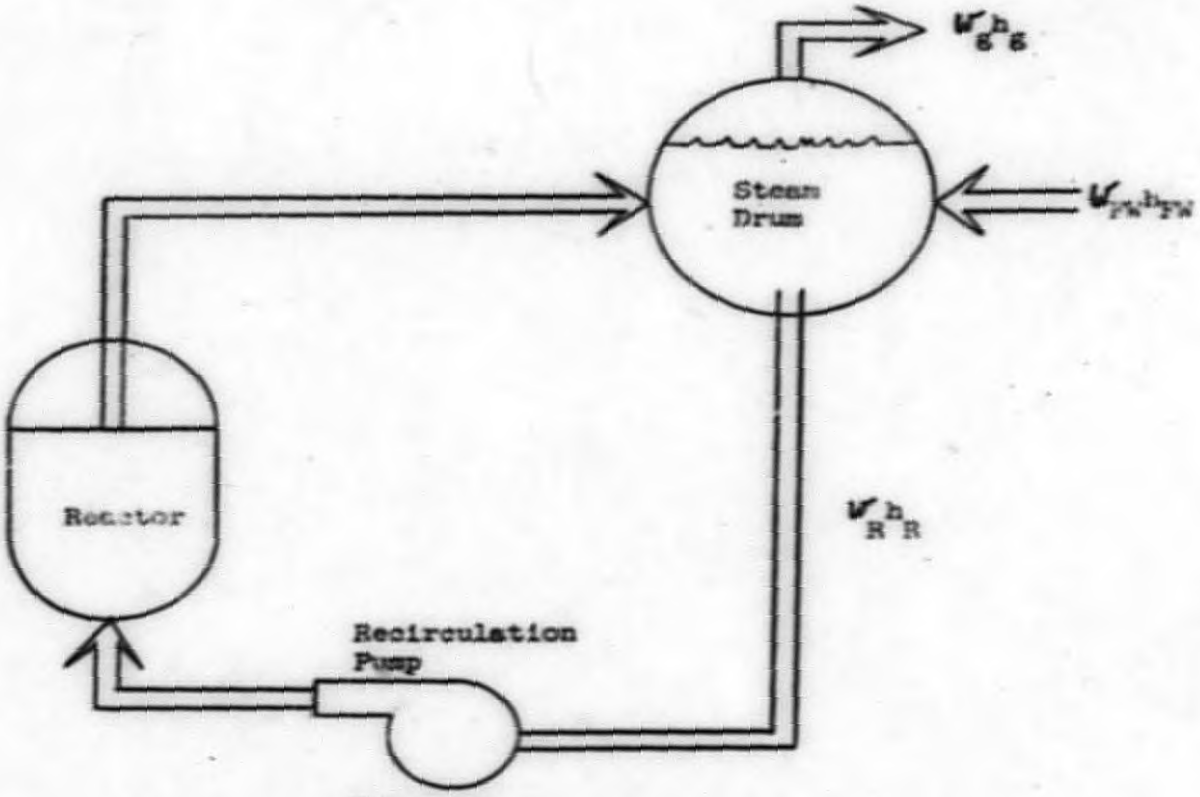

Figure 2
Schematic Diagram of Pressure Rate Model

$$\dot{P} = \frac{Q + W_{FW} h_{FW} - W_g h_g}{D_1}$$

Or in per unit values:

$$\dot{P}^* = \frac{\left[\frac{Q_o}{P_o}\right] Q^* + \left[\frac{W_{FW_o} h_{FW_o}}{P_o}\right] W_{FW} h_{FW}^* - \left[\frac{W_{g_o} h_{g_o}}{P_o}\right] W_g h_g^*}{D_1} \quad (11)$$

Equation (11) evaluated for the 50 MWe Consumers core at rated conditions:

$$\dot{P}^* = 0.0195\, Q^* + 0.00694\, W_{FW} h_{FW}^* - 0.0264\, W_g h_g^* \quad (12)$$

Pressure Voids

The pressure voids transfer function is a linear relationship which describes the steam volume within the core (U_p^*) as a function of the time rate of pressure change in the nuclear steam supply system (P^*). This relationship is

based upon the same considerations that were employed in the derivation of the pressure rate transfer function. The boundary conditions for this model, however, are limited to the reactor core only.

Solving for the core steam flow rate (w_g^*) versus steam supply system pressure rate ($\dot{P}^*$):

$$w_g^* = -\frac{D_2}{\left[\frac{h_{fg_o} v_{g_o}}{v_{f_o}}\right]\left[\frac{w_{g_o}}{P_o}\right]} \dot{P}^*$$

WHERE:

$$D_2 = M_g\left[\frac{\Delta h_g}{\Delta P} - \frac{h_{fg}\,\Delta v_g}{v_{fg}\,\Delta P}\right] + M_f\left[\frac{\Delta h_f}{\Delta P} - \frac{h_{fg}\Delta v_g}{v_{fg}\Delta P}\right]\frac{V_c}{J} \quad (13)$$

assuming for small changes that steaming rate variations are equivalent to steam volume variations (a conservative assumption) and rearranging:

$$\frac{u_p^*}{\dot{P}^*} = -\frac{D_2}{\left[\frac{h_{fg_o} v_{g_o}}{v_{s_o}}\right]\left[\frac{w_{g_o}}{P_o}\right]} \quad (14)$$

Equation 14 evaluated for the Consumers 50 MWe core at rated conditions

$$\frac{u_p^*}{\dot{P}^*} = -5.3 \quad (15)$$

Saturation and Subcooling

The saturation and subcooling transfer functions constitute a linear representation which relates pressure rate effects ($\dot{P}^*$) to energy ($w_R \Delta h_s^*$) which must be supplied by the core to overcome inlet subcooling. Effects of recirculation temperature variations are realized through the enthalpy h_R^*.

From the steam tables it is found for 1050 psia ± 100 psi: $\Delta h_g = 0.15\ \Delta P$ relating this expression to $\dot{P}^*$:

$$\frac{h_f^*}{\dot{P}^*} = \frac{0.15\ P_o}{(S)\ h_{f_o}} \quad (16)$$

Subcooling is defined:

$$h_s = h_f - h_R$$

or, in per unit values:

$$\frac{h_{so}}{h_{fo}} h_s^* = h_f^* - \frac{h_{Ro}}{h_{fo}} h_R^* \qquad (17)$$

Energy in the subcooling can be expressed as $W_R h_s^*$. If W_R is assumed constant:

$$W_R h_s^* = h_s^* \qquad (18)$$

If no variation in h_R^* is added at the summation point (see Figure 1) equations (16), (17) and (18) can be combined:

$$\frac{W_R h_s}{\dot{P}^*} = \frac{(0.15) P_o}{(S) h_{so}} \qquad (19)$$

Equation (19) evaluated for the Consumers 50 MWe core at rated conditions

$$\frac{W_R h_s^*}{\dot{P}^*} = \frac{10.5}{(S)} \qquad (20)$$

Pressure Reactivity

The pressure reactivity transfer function is a linear relationship which describes the excess reactivity (ΔK_P) due to steam volume changes (U_P^*) within the core that are caused by pressure variations. This is a transport relation which averages the steam volume due to flashing or collapse within the core and assigns a void worth of reactivity to that average.

Referring to Appendix B for the transport relation and using a void worth of $4.50:

$$\frac{\Delta K_P}{U_P^*} = \frac{4.5 \frac{T_c}{2}(S)\left(1 + \frac{T_c S}{8}\right)}{\left(1 + \frac{T_c S}{4}\right)^2} \qquad (21)$$

Equation (21) evaluated for the Consumers 50 MWe core at rated conditions:

$$\frac{\Delta K_P}{U_P^*} = \frac{0.652(S)[1+0.0362(S)]}{[1+0.0725(S)]^2} \quad (22)$$

Heat and Subcooling Reactivity

The heat and subcooling reactivity transfer function is a linear relationship which describes the excess reactivity ($\Delta K_Q + \Delta K_h$) due to steam volume changes (U_Q, U_h^*) within the core that are caused by reactor heat and recirculation loop subcooling variations. This is a transport relation which averages the core steam volume due to the above two influences and assigns a void worth of reactivity to that average.

Referring to Appendix B for the transport relation and using a void worth of $4.50:

$$\frac{(\Delta K_Q + \Delta K_h)}{U_{Q,h}^*} = \frac{4.5}{1 + \frac{T_c S}{2} + \frac{T_c^2 S^2}{12}} = \frac{4.5}{1 + 2\xi_{S3} T_q S + T_q^2 (S)^2} \quad (23)$$

The numerical value of Tc in the above equations must be determined for each operating condition of the reactor if this relationship is to be used. This restriction, like that imposed upon the hydrodynamic analysis arises from the fact that the transfer function as it appears in Equation (23) is a linearized simplification of a non-linear model.

METHOD OF ANALYSIS

The analytical model described in the preceding section and pictorially represented in Figure 1 was applied to the Consumers reactor design for a stability investigation of the plant at various power levels and for the purpose of predicting the operating flux noise level. The stability investigation was accomplished by performing a frequency-phase shift analysis (Bode analysis) on the analytical model. The power conditions at which stability was investigated were 50%, 100% and 125% rated power for the 50 MWe core and 100% rated power for the 75 MWe core. Flux noise predictions were formulated by an estimating scheme introduced in an analysis of the Vallecitos Boiling Water Reactor core #1-C[9]. Operating flux noise predictions were made for the Consumers 50 MWe core at 100% rated power.

The following describes the analysis procedures which were used in each of the investigation points mentioned above.

Stability Analysis - 50 MWe Core at 100% Rated Power

Solutions for each of the transfer functions represented in the analytical model (see Figure 1) were obtained for this reactor condition and were examined for their individual contribution to system stability. It was found, upon first examination, that:

A. The Doppler coefficient produced a negative feedback effect which made an insignificant contribution to the magnitude of the reactor kinetics transfer function at the frequencies of interest. Moreover, it had a phase shift contribution which diminished the 90° phase lag induced by the integrator (1/s) term of the reactor kinetics. Therefore, omitting the effect of the Doppler coefficient will lead to a conservative stability analysis.

B. The effect of pressure induced subcooling ($W_R h_s^*$), although a positive feedback mechanism was negligible at the frequencies of interest ($W_R h_s^*$ less than 5% of Q^*).

The final form of the analytical model used for this portion of the stability analysis was obtained by neglecting the above two influences and omitting the external excitations of Figure 1 $W_g h_g$, $W_{FW} h_{FW}$, and h_R^*. Figure 3 is a block diagram of the resulting model applied to the 50 MWe core at 100% rated power.

This model was analyzed in the following steps:

1. The magnitude and phase shift response with frequency was plotted for the forward transfer function (G) of the reactor-recirculation loop (Reactor Kinetics and Fuel Model). See Figure 6.

2. The magnitude and phase shift response with frequency was plotted

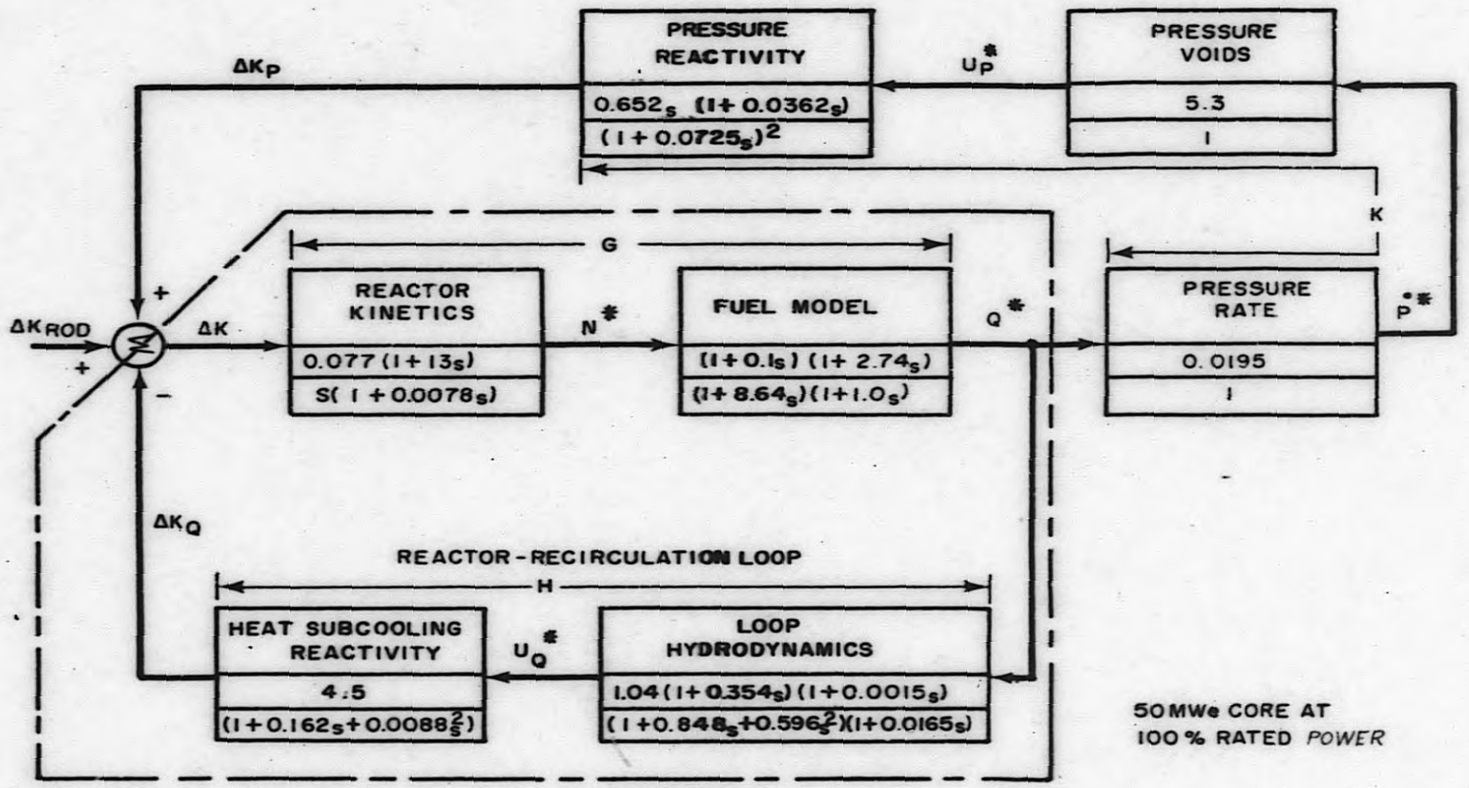

FIGURE 3

CONSUMERS BIG ROCK STABILITY ANALYSIS REDUCED BLOCK DIAGRAM

for the feedback transfer function (H) of the reactor-recirculation loop (loop hydrodynamics and heat-subcooling reactivity). See Figure 7.

3. The preceding two plots were used to obtain the open-loop response (GH), including gain and phase margins, of the reactor-recirculation loop. See Figure 8.

4. The closed loop response G/(1 + GH) of the reactor-recirculation loop was obtained from 2 and 3 above by the use of a "Nichols" chart.[10] See Figures 9 and 10.

5. The magnitude and phase shift response with frequency was plotted for the positive feedback transfer (K) of pressure-induced reactivity (pressure rate, pressure voids and pressure reactivity). See Figure 11.

6. The total open loop response GK/(1 + GH) including stability margins, was obtained from 4 and 5 above. See Figure 12.

Stability Analysis - 50 MWe Core at 50% and 125% Rated Power and 75 MWe Core at 100% Rated Power

It was found during the 100% rated power - 50 MWe core analysis that the positive feedback of pressure-induced reactivity (K - see Figure 11) did not have sufficient gain at the frequencies of interest to be of significant value in the determination of system stability. In other words, the system stability characteristics for the Consumers reactor are dominated by the response of the reactor-recirculation loop. Moreover, for the purposes of this study no additional information about stability limits is achieved by including the pressure effect. Therefore, the analytical model can be further simplified and the three remaining points for stability investigation can be analyzed on the basis of the reactor-recirculation loop alone.

A block diagram of the resulting analytical model for the 50% rated power - 50 MWe core, the 125% rated power - 50 MWe core, and the 100% rated power - 75 MWe core is shown in Figure 4. This model was analyzed in the following steps:

1. The magnitude and phase shift response with frequency was plotted for the feedback transfer (H) of the reactor-recirculation loop (loop hydrodynamics and heat-subcooling reactivity). See Figures 13, 15 and 17.

2. The plots calculated above were combined with the forward transfer (G) which remains identical for all of the reactor conditions (see Figure 6) and open loop responses (GH), including gain and phase margins were obtained. See Figures 14, 16 and 18.

Noise Analysis - 50 MWe Core at 100% Rated Power

Neutron flux noise occurring while a BWR is operating at some equilibrium position is believed to be attributable to randomly varying voids within the core which may be considered, for analytical purposes, to be due to fluctuations in the

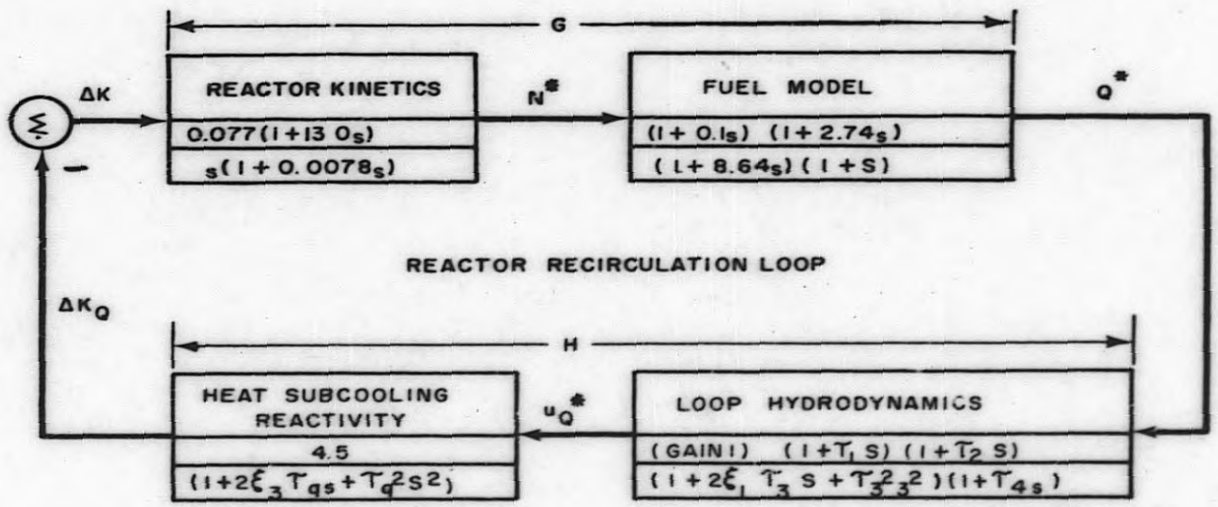

	$2\xi_3 T_q$	T_q^2	GAIN 1	T_1	T_2	$2\xi_1 T_3$	T_3^2	T_4
50 MWe CORE - 50% RATED POWER	0.189	0.0119	0.784	0.66	0.0009	0.954	0.868	0.0137
50 MWe CORE -100% RATED POWER	0.162	0.0088	1.04	0.354	0.0015	0.848	0.596	0.0165
50 MWe CORE-125% RATED POWER	0.154	0.0079	0.704	0.357	0.0019	0.604	0.519	0.0179
75 MWe CORE-100% RATED POWER	0.253	0.0213	1.12	0.257	0.0024	0.843	0.734	0.0180

FIGURE 4

CONSUMERS BIG ROCK STABILITY ANALYSIS REACTOR-RECIRCULATION LOOP BLOCK DIAGRAM

inlet water temperature. These temperature fluctuations, acting as noise excitations, are "filtered" (i.e., changed in its frequency spectrum) before becoming a reactivity noise.[11] It is suggested that this filtering device is the time-dependent response of parallel flow channel mechanisms within the reactor core. A qualitative evaluation of the effect of design conditions upon probable flux noise level in the Consumers reactor was obtained by application of the above logic. The resulting simplified analytical model is pictorially represented in Figure 5. The reader will notice, at first glance, that the model is open loop in character. That is, no account is shown for the seemingly possible effect of flux noise (N^*_{noise}) upon noise excitation (α^*). The omission of a feedback mechanism was made deliberately, however, for it was found that the fuel model was effectively a low pass filter which blocked the high frequency response of the parallel flow channel hydrodynamics.

The flux noise analysis was conducted on the Consumers 50 MWe core at 100% rated power. Two different fuel element orificing configurations were studied for this reactor condition:

1. Unorificed hot channels in the center of the core.

2. Orificed hot channels in the center of the core - the orificing being equivalent to 5 psi additional ΔP across the element.

Condition 2., above, could be physically realized by just merely raising 5 psi the entire core pressure drop scheme of configuration 1. and, at the same time holding the total core flow constant. It was the authors' intent, by investigating these two geometries, to qualitatively evaluate the effect of core orificing design upon flux noise.

The analytical models for conditions 1. and 2., above, were obtained by application of the hydrodynamic analysis (see Appendix A) to the described parallel flow channel mechanism. A block diagram of this model is presented in Figure 5. This model was analyzed in the following steps:

1. The magnitude and phase shift response with frequency was evaluated and plotted for the transfer of flux noise (N^*_{noise}) from excitation (α^*). See Figure 19.

2. The peak gain of this transfer due to parallel flow channel hydrodynamic response and its corresponding frequency was determined from the plot.

3. The flux noise prediction was obtained by assuming a cyclic fluctuation in the subcooling excitation (at the hydrodynamic resonant frequency) equivalent to a $\pm$ 0.1°F variation in the inlet recirculation water.

It should be pointed out that this noise analysis is not considered exact. No account has been taken for neutron coupling or the smoothing of individual fuel

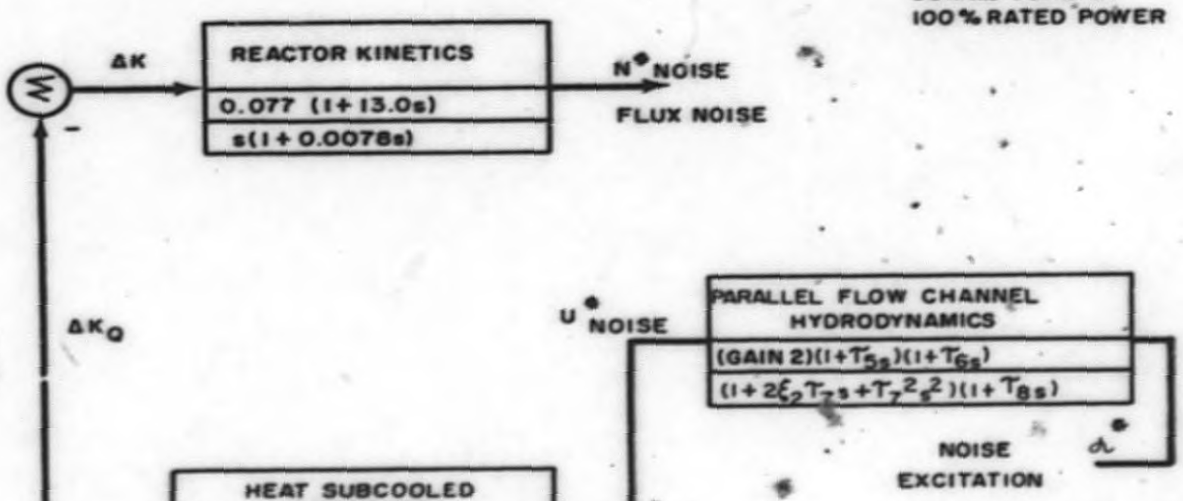

	T_8	T_7^2	$2\xi_2 T_7$	T_6	T_5	GAIN 2	T_q^2	$2\xi_3 T_q$
NO INLET ORIFICING	0.0042	0.0066	0.0097	0.0004	0.025	0.213	0.00875	0.162
5 PSI INLET ORIFICING	0.0040	0.0068	0.0520	0.0004	0.017	0.154	0.00875	0.162

FIGURE 5
CONSUMERS BIG ROCK PERFORMANCE ANALYSIS BLOCK DIAGRAM

element flux noise by adjacent elements and the parallel flow channel coupling has been approximated (see Appendix A). Furthermore, the exact nature and magnitude of the noise disturbance or driving excitation that occurs within the reactor is not known. The analysis does include, however, the fundamental principles which are believed capable of describing the flux noise mechanism: a) The fuel element is considered to be a hydrodynamic amplifier with a definite frequency response, b) this amplifier can be driven with disturbances in any of several physical quantities which affect flow-subcooling, pressure, heat, geometry, etc. (a subcooling excitation was considered for this analysis), c) these disturbances, acting through the hydrodynamic amplifer, cause changes in the moderator density, d) changes in moderator density are related to fluctuations in reactivity, and finally, e) fluctuations in reactivity cause variations in neutron flux level. The authors are confident about the qualitative value of this noise analysis. Recent measurements of flux noise in the Vallecitos Boiling Water Reactor[19] tend to strengthen this confidence. The quantitative value of this simplified analysis is yet to be determined.

RESULTS

The results of the Big Rock stability analysis are summarized below, instability being indicated by zero phase and gain margin.

Reactor Condition	Phase Margin	Gain Margin
50 MWe core at 50% rated power	66°	15 db
50 MWe core at 100% rated power	68°	14 db
50 MWe core at 125% rated power	87°	11 db
75 MWe core at 100% rated power	28°	6 db

The 50 MWe core is seen to be stable at all power levels investigated. The stability margins of the 75 MWe core, although somewhat less than those of the 50 MWe core, conservatively indicate that no serious stability problems will be encountered in this mode of operation.

The results of the noise performance analysis for the 50 MWe core at 100% rated power, based on an arbitrary disturbance in inlet subcooling, are given below:

Core Condition	Maximum Predicted Noise Level
Unorificed fuel elements in the center of the core	7.45% peak to peak
Fuel elements in the center of the core with 5 psi inlet orificing	1.35% peak to peak

Fuel element inlet orificing has a significant damping effect upon parallel flow channel mechanisms which in turn, increase the attenuation of reactor flux noise. If the center fuel elements of the Big Rock core are not orificed for the initial startup and the resulting flux noise is objectionable, a remedy is indicated -- raise the single-phase orifice pressure drop over the entire core.

All of the results obtained in this study were obtained by assuming that the rate of change of reactivity due to 100% change in voids for the given power operating condition is $4.50. This is conservatively high for all cases considered, and in particular for partial rated power conditions.

In the operational phase of the R&D program a stability testing program will be conducted to assure operational stability and to evaluate the accuracy or degree of conservatism inherent in this analysis.

The following is a detailed discussion of the results presented above:

50 MWe Core at 100% Rated Power

The frequency response plot of the combined reactor kinetics and heat diffusion transfer functions (G - see Figure 3) is presented in Figure 6. It is observed that the magnitude at the low end of the frequency spectrum begins at a value slightly less than one (0 db) and continually decreases with increasing frequency. This early appearance of gain attenuation in the frequency spectrum reflects low fuel thermal conductivity contribution. The phase shift response is observed to be comparatively flat throughout the frequency range (30 - 70° lag).

The Bode' plot of the combined loop hydrodynamics and heat-subcooling reactivity transfer function (H) is presented in Figure 7. The flow loop hydrodynamics is characterized in this plot by the low frequency gain attenuation which occurs at about 1 radian/second. The higher frequency gain attenuation which "cuts off" at about 10 radians/second is a manifestation of the heat-subcooling reactivity transfer function. It is interesting to note that the two above effects are separated by about a decade in frequency. This can be explained by recognizing that the natural period of the loop hydrodynamics is roughly proportional to the entire two-phase flow transit time (core and risers) while the natural period of the heat-subcooling reactivity is proportional to the flow transit time through the core only. It should be noted that the loop hydrodynamics transfer function (Equation 8) contains a quadratic term which will cause, for underdamped systems, a characteristic resonant "hump" at the loop natural frequency. It can be seen from inspection of Figure 7 that no such resonance occurs. Therefore, the response of the Big Rock hydrodynamic system at this power level is, by itself, very well damped.

Figure 8 is an open loop plot of the reactor-recirculation loop magnitude and phase shift response to frequency (GH). It is this plot which describes stability margins for the reactor-recirculation loop portion of the total feedback network. This plot was obtained by summing the curves of Figures 6 and 7. It can be seen from Figure 8 that the reactor-recirculation loop is stable with a 68° phase margin and a 14 db gain margin. These stability margins compare favorably with conventional feedback system design criteria.

The closed loop frequency response of the reactor-recirculation loop G/(1 + GH) is shown in Figure 10. This plot was obtained by the use of the "Nichols" chart illustrated in Figure 9. It is this closed loop response of the reactor-recirculation loop which combines with the pressure rate, pressure voids, and pressure reactivity path (K) to form a positive feedback network in ΔK (see Figure 3). It can be observed from Figure 10 that the magnitude of this closed loop response is always -10 db or less. The low gain of this response is quite decisive, as will be seen later, in attenuating the effect of positive feedback.

The frequency response characteristic of pressure rate, pressure voids, and pressure reactivity (K) is illustrated in Figure 11. The steady-state magnitude of this combined transfer function is composed of contributions from all three of its component models. Its frequency response, on the other hand, is determined

solely by the pressure reactivity model. The initial positive slope of the magnitude reflects the differentiator (s is the numerator) in the pressure reactivity model. The flattening of the magnitude response at about 10 radians/second is caused by the combined effect of the single time constant numerator and the double time constant denominator of the pressure reactivity model. It should be pointed out that the magnitude of this response does not exceed -5 db.

Figure 12 is an open loop plot of the total loop magnitude and phase shift response to frequency GK/(1 + GH). This is a positive feedback network. It can be seen from this illustration that at no frequency does the magnitude exceed -30 db. Since unstable operation requires a minimum of unity gain (0 db) the positive feedback loop does not introduce instability in this system. The total feedback loop is seen to be very stable -- even greater in degree than was indicated by the previous analysis of the component reactor-recirculation loop.

50 MWe Core at 50% Rated Power

The frequency response plot of the combined loop hydrodynamics and heat-subcooling reactivity transfer functions (H - see Figure 4) for the 50 MWe core at 50% rated power is presented in Figure 13. The dashed lines shown in this figure are the corresponding responses evaluated for the 100% rated power -- 50 MWe core case (see Figure 7). It is observed from this comparison that there is very little difference exhibited between the responses of these two systems. A close inspection of the magnitude comparison shows a very slight "slow down" in the frequency response of the 50% power case. This should be expected because experiments have generally shown that the natural frequency of a given two-phase loop increases with power.

Figure 14 is an open loop plot of magnitude and phase shift versus frequency for the 50% rated power -- 50 MWe core reactor-recirculation loop. The dashed lines shown in this figure are the corresponding responses of the 100% rated power condition (see Figure 8). This plot was obtained by summing the reactor kinetics and heat diffusion transfer function (G - see Figure 6) and the loop hydrodynamics and heat-subcooling transfer function (H) of Figure 13. The linearized G transfer function is assumed not to be affected by normalized power level. Therefore, the response differences seen in this open loop plot of Figure 14 are just a reflection of the differences in H mentioned above. The same discussion and comments apply. The 50% rated power -- 50 MWe core reactor-recirculation loop is seen to be stable with a 66° phase margin and a 15 db gain margin. These margins are essentially the same as were found at rated power.

50 MWe Core at 125% Rated Power

The frequency response plot of the combined loop hydrodynamics and heat-subcooling reactivity transfer function (H) for the 50 MWe core at 125% power is presented in Figure 15. The dashed lines shown in this figure are the corresponding responses of the 100% power condition. The magnitude responses for these two

power conditions are again observed to be almost identical. A close inspection of the magnitudes shows, however, that the frequency response is slightly faster in the 125% power condition. This trend with power is the same as was discussed in the 50% rated power case. The phase shift curve of the 125% power condition is seen to be somewhat different than in the 100% power condition. This difference occurs between about 0.5 to 5.0, radians/second frequency, and brackets the natural frequency of the loop hydrodynamics model. The quadratic equation in this model, which strongly influences the natural frequency, has a smaller damping ratio in the 125% power condition than it did for the 100% power condition (see Figure 4). This results in the hydrodynamic model phase shift curve of Figure 15 being bent into a steeper "S" shape within the affected frequency band.

Figure 16 is an open loop plot of magnitude and phase shift versus frequency for the 125% rated power reactor-recirculation loop. It is observed from this figure that this reactor condition is stable with an 87° phase margin and an 11 db gain margin. The phase margin, which is larger than that for rated conditions by about 20°, and the gain margin, which is less by about 3 db, demonstrate a combination of results characteristic of a stable but more underdamped response system. The phase margin is greater because the lower quadratic damping ratio mentioned above depresses the phase lag in the region of the gain crossover.

75 MWe Core at 100% Rated Power

The frequency response plot of the combined loop hydrodynamics and heat-subcooling reactivity transfer function (H) for the 75 MWe core at rated power is presented in Figure 17. The dashed lines shown in this figure are the corresponding responses of the same transfer function evaluated for the 100% rated power -- 50 MWe core condition. A comparison of the magnitude curves for these two reactor conditions presents some interesting results:

A. The magnitudes are essentially the same up to a frequency of about 2 radians/second.

B. Beyond 2 radians/second the 75 MWe condition attenuates more rapidly and finally establishes a consistently lower gain than the 50 MWe condition from about 20 radians/second.

It was mentioned during the discussion of the rated power -- 50 MWe core condition that this transfer function (H) is composed of a low frequency response model (loop hydrodynamics) and a high frequency response model (heat-subcooling reactivity). Therefore, observations A. and B., above, can be restated in the following manner:

A. The loop hydrodynamics of the 75 MWe condition is essentially the same as the 50 MWe condition.

B. The heat-subcooling reactivity model, which is proportional to core flow transient time, has a significantly lower frequency in the 75 MWe condition than it does in the 50 MWe condition.

The primary physical difference between the 75 MWe reactor configuration and the 50 MWe reactor configuration is one of increased core flow area. In the 75 MWe condition the additional power is achieved by adding more elements to core. The total recirculation flow, heat input per fuel element, downcomer flow area and the riser flow area remain essentially the same. Also, even though the gross power output of the core is greater, the void content of the risers remains about the same. This is explained by the increase in system pressure from 1000 psia to 1500 psia. The core flow area, however, is increased appreciably. This increased core flow area results in a lower frequency response of the heat-subcooling reactivity model while the loop hydrodynamics model is dominated by the risers and is not appreciably affected by the increased core flow area.

The phase lag of the H transfer function for the 75 MWe reactor condition is seen to be greater than in the 50 MWe condition. This is primarily caused by the lower frequency contribution of the heat-subcooling reactivity model mentioned above.

Figure 18 is an open loop plot of magnitude and phase shift versus frequency for the 100% rated power -- 75 MWe core reactor-recirculation loop. It is observed from this plot that this reactor condition is stable with a 28° phase margin and a 6 db gain margin. The reduction in the 75 MWe reactor's stability margins can be attributed largely to the larger flow area of the core (a lower frequency response of the heat-subcooling reactivity model). It causes the phase lag to be greater in the region of gain crossover and the gain to be greater in the region of 180° phase lag.

Flux Noise Performance Analysis

50 MWe Core at Rated Power

A plot of magnitude versus frequency for the flux noise from noise excitation based on the transfer function of Figure 5 is presented in Figure 19. This transfer function is an open loop combination of the parallel flow channel hydrodynamic model, the heat-subcooling reactivity model, and the reactor kinetics model. It was evaluated for the rated power -- 50 MWe at two different conditions:

A. Unorificed hot channels in the center of the core.

B. Orificed hot channels in the center of the core -- the orificing being equivalent to 5 psi additional ΔP across the element.

The qualitative effect of channel inlet orificing can be determined by a comparison of the two magnitude versus frequency curves shown in Figure 19. The noise transfer function containing an unorificed hot channel is observed to display a characteristic resonant peak in its frequency response. The orificed transfer function, however, does not display this resonant character. Its frequency behavior is typical of a near criticality damped system response, with a "cut off" frequency occurring approximately at the same frequency as the resonant peak of the unorificed case. It is evident from the foregoing observations that channel

inlet orificing has a significant influence upon this transfer function. It is seen that the frequency response of magnitude is attenuated by an increase in channel inlet orificing.

Since changes in channel inlet orificing have no effect upon the reactor kinetics model or the heat-subcooling reactivity model (see Figure 5), it can be concluded that the above mentioned attenuation is a measure of the hydrodynamic model's response to single-phase pressure losses; i.e., an increase in channel inlet orificing tends to damp transients in the two-phase flow region. This trend can be explained by the following reasoning:

1. Increasing the inlet orificing of a fuel element, or channel, raises the single-phase flow losses of that channel.

2. Increased single-phase losses in a channel damp single-phase transients.

3. If single-phase transients are damped, then by virtue of continuity of mass within the flow path, the two-phase transients in a near constant pressure system will also be damped.

The exact degree, to which orificing damps flux noise is difficult to assess. Presently available information does not provide conclusive evidence about the nature, amplitude or frequency spectrum of the noise excitation. It is believed, however, that a realistic qualitative evaluation of the damping effect can be obtained by comparing the maximum magnitudes of each curve shown in Figure 19. In essence, this analysis technique implies that it is not necessary to know the origin of excitation. We recognize that the parallel channel mechanism is an amplifier which will transmit any disturbance that affects the hydrodynamics of the system. In this study a subcooling disturbance was postulated. However, even if the actual noise excitation proves to be something other than subcooling the relative responses of the amplifier will remain the same. This analysis technique also implies that the amplitude and frequency spectrum of the noise excitation is a modified white noise structure; i.e., all frequencies are present and the amplitude is the same for each frequency.

The qualitative difference between the two orificing schemes was found by employing the technique outlined above. It is observed from Figure 19 that the maximum magnitude difference between the two curves is about 15 db. This means that the amplitude of flux noise would be 15 db or about 5-1/2 times greater without orificing the fuel element inlets. It should be noted that any additional orificing in excess of 5 psi, while it would attenuate noise level some, it would not continue to reduce the noise at the same rate as the first 5 psi. This is, of course, because the frequency response has already been essentially flattened with 5 psi orificing.

Somewhat less confidence is placed in the quantitative properties of the flux noise model than is placed in its qualitative properties. This statement, of course, follows logically. As was mentioned before, the exact disturbance which causes flux noise is not known. Furthermore, even if the nature of this disturbance were known, it would be difficult, at this time, to determine its amplitude.

It was assumed, for the purposes of this study, that the disturbances are small temperature variations in the inlet flow to the channels. This assumption was made primarily in an effort to achieve a limited quantitative appreciation for the noise mechanism by relating the flux noise to a fluctuation in a familiar quantity (inlet flow temperature variations). The procedure which was used to accomplish this limited quantitative evaluation was as follows:

a. The nature of the driving excitation for flux noise was assumed (temperature variation in the inlet flow).

b. A conservative amplitude was assigned to this excitation's modified white noise spectrum ($\pm$ 0.1°F temperature variations were used in this analysis). It is believed that this disturbance magnitude would not be exceeded during normal operation of the power plant being considered.

c. The temperature variation -- assumed in b., above, was related to a subcooling fluctuation.

d. This subcooling fluctuation was applied to the noise transfer function (N^*_{noise}/α^*) and a prediction was made of the noise level and predominant frequency.

It is believed that noise predictions based on the foregoing procedure will produce values higher than actual.

The following estimates of flux noise were made for the two curves shown in Figure 19 by using the above procedure:

Hot channel with inlet orificing	7.45% peak to peak flux noise at 2 cps predominant frequency
Hot channel with 5 psi inlet orificing	1.35% peak to peak flux noise with flat frequency spectrum from 0.0016 - 20 cps. Attenuation at 40 db per decade beyond 20 cps.

It should be mentioned again that this is by no means intended to be a complete noise analysis. The flux noise which will be measured both in-core and out-of-core will display the weighted integrated noise contributions of all of the channels within the reactor core. This analysis investigated the hot channel contribution to flux noise only. The hot channel contribution, however, is the strongest of any single element within the core. Therefore, from a quantitative standpoint, the above flux noise predictions should be considerably higher than actual. In any event, from a qualitative standpoint, if the center fuel elements are not orificed for the initial reactor startup and the resulting flux noise is objectionable, a remedy is indicated -- raise the single-phase orificing of the entire core.

FIGURE 6
FREQUENCY RESPONSE CHARACTERISTICS
OF REACTOR KINETICS AND HEAT DIFFUSION- $Q/\Delta K(G)$

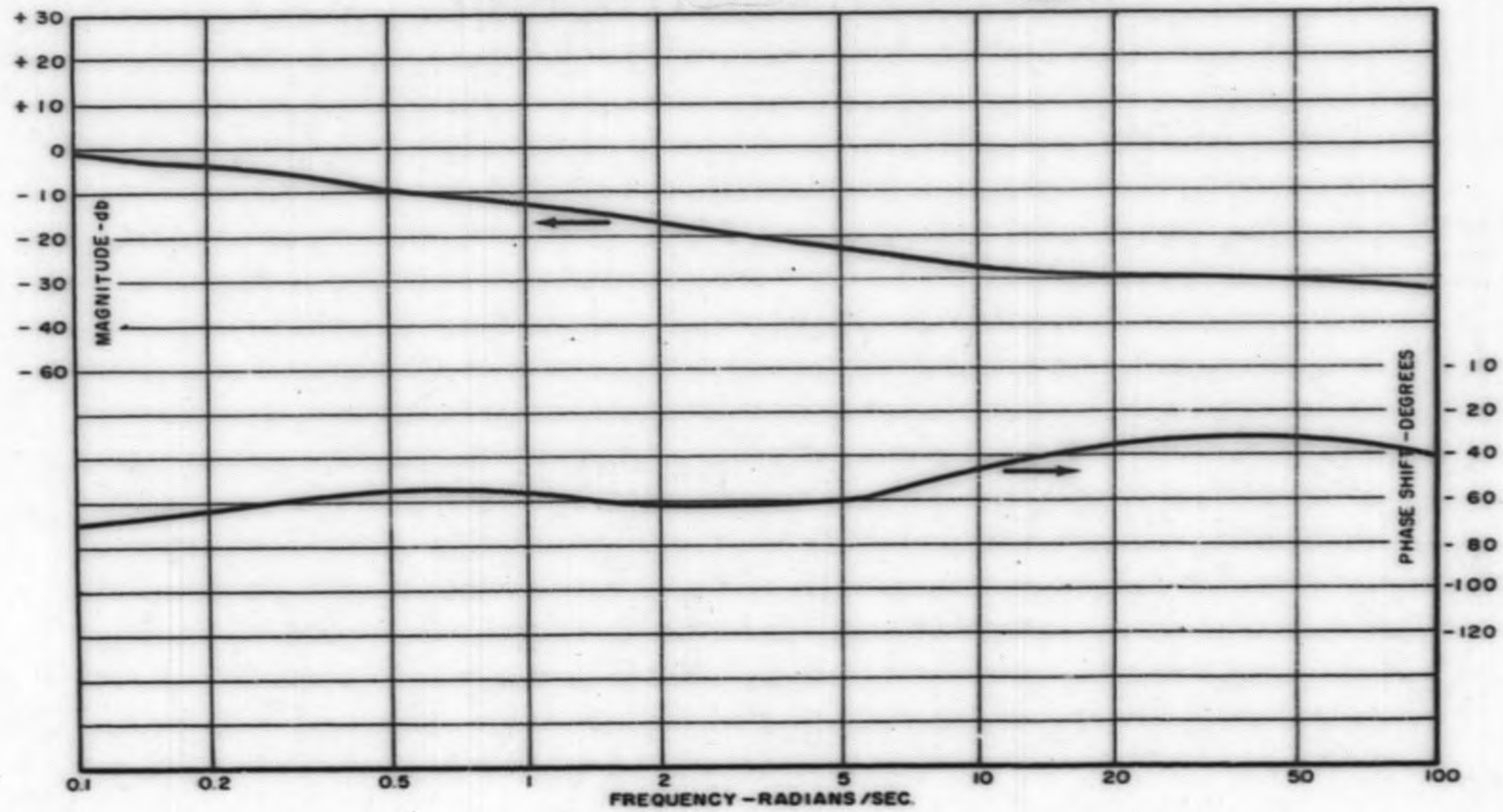

FIGURE 7

FREQUENCY RESPONSE CHARACTERISTIC OF THE FLOW LOOP HYDRODYNAMICS — $\frac{\Delta K_e}{\alpha^o}(H)$

RATED CONDITIONS
50 MW CORE
VOID WORTH — $ 4.50

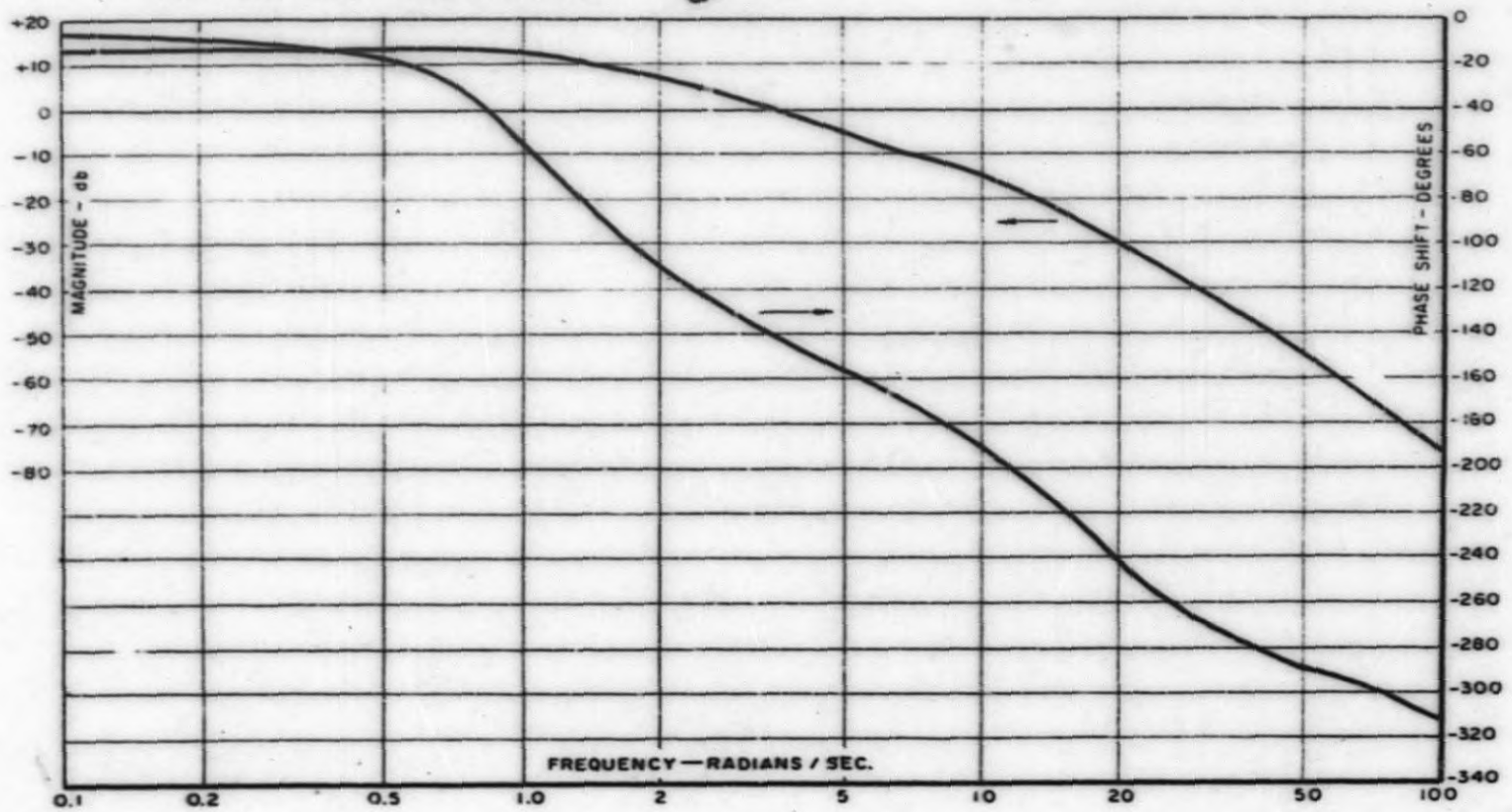

FIGURE 8

FREQUENCY RESPONSE CHARACTERISTIC OF THE REACTOR-RECIRCULATION LOOP — $\frac{\Delta K_e}{\Delta K}$ (OPEN LOOP) (GH)

RATED CONDITIONS
50 MW CORE
VOID WORTH — $ 4.50

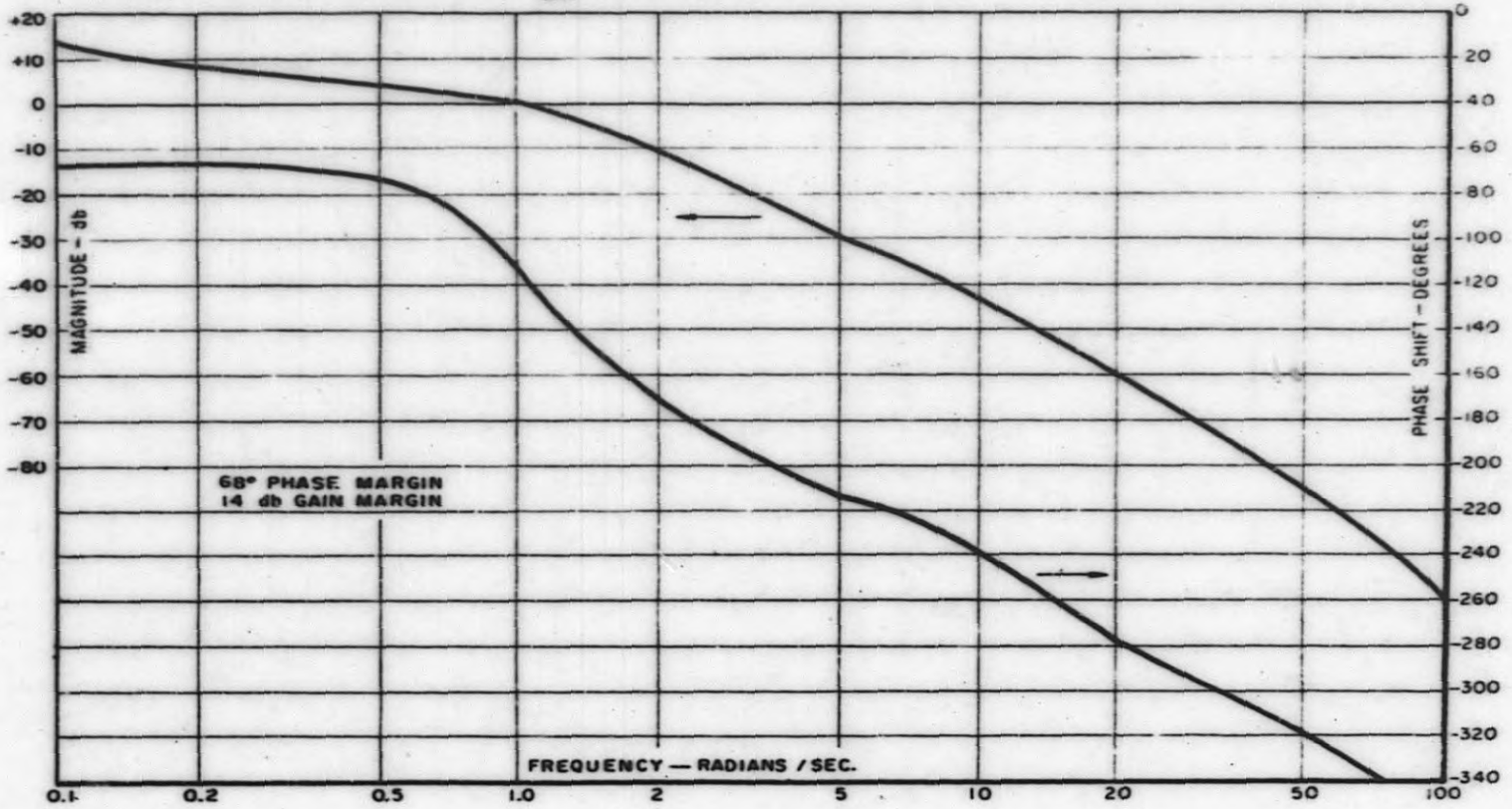

FIGURE 8
FREQUENCY RESPONSE CHARACTERISTIC OF THE
REACTOR-RECIRCULATION LOOP — $\frac{\Delta K_e}{\Delta K}$ (OPEN LOOP) (GH)

RATED CONDITIONS
50 MW CORE
VOID WORTH — $ 4.50

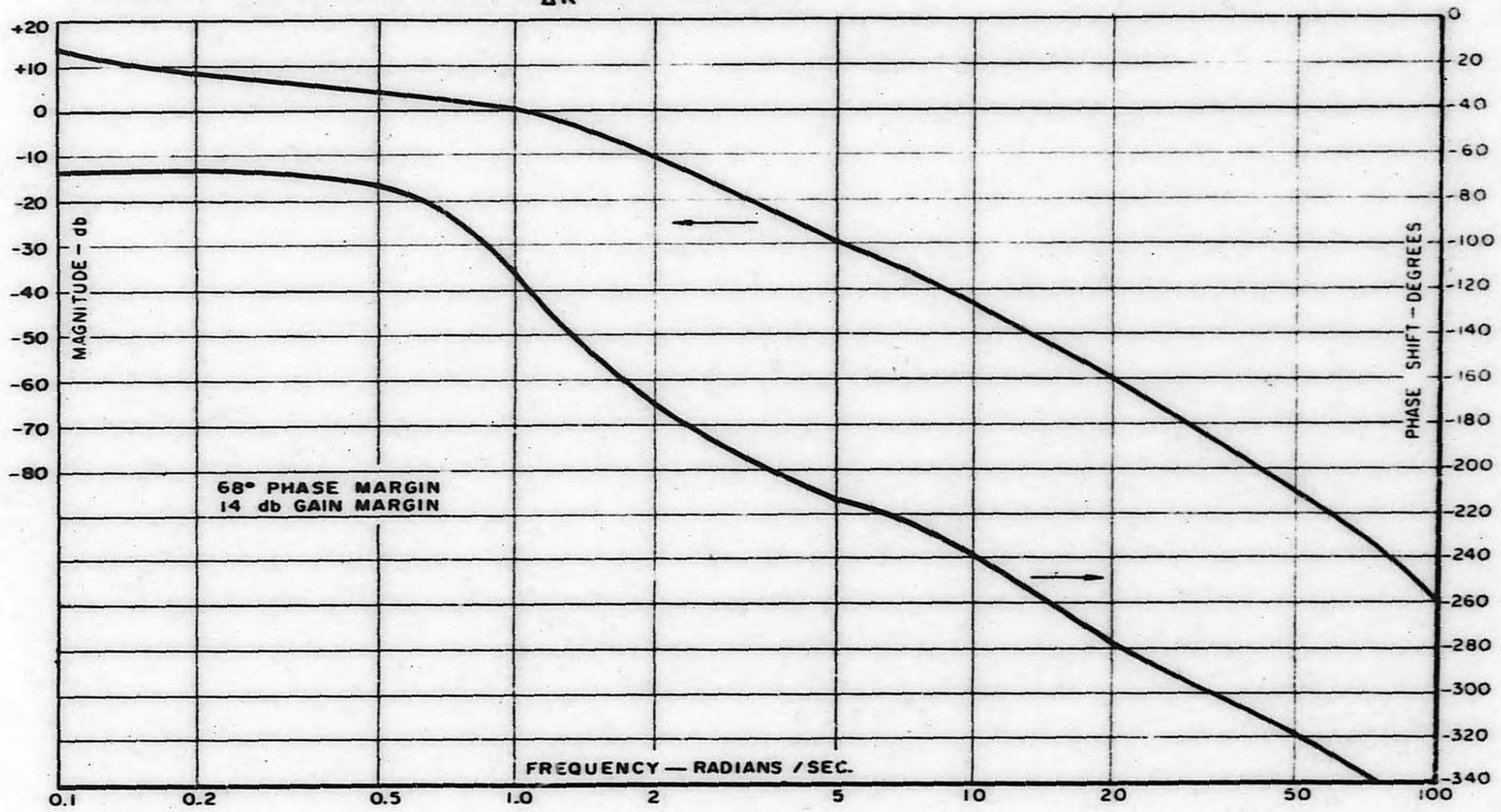

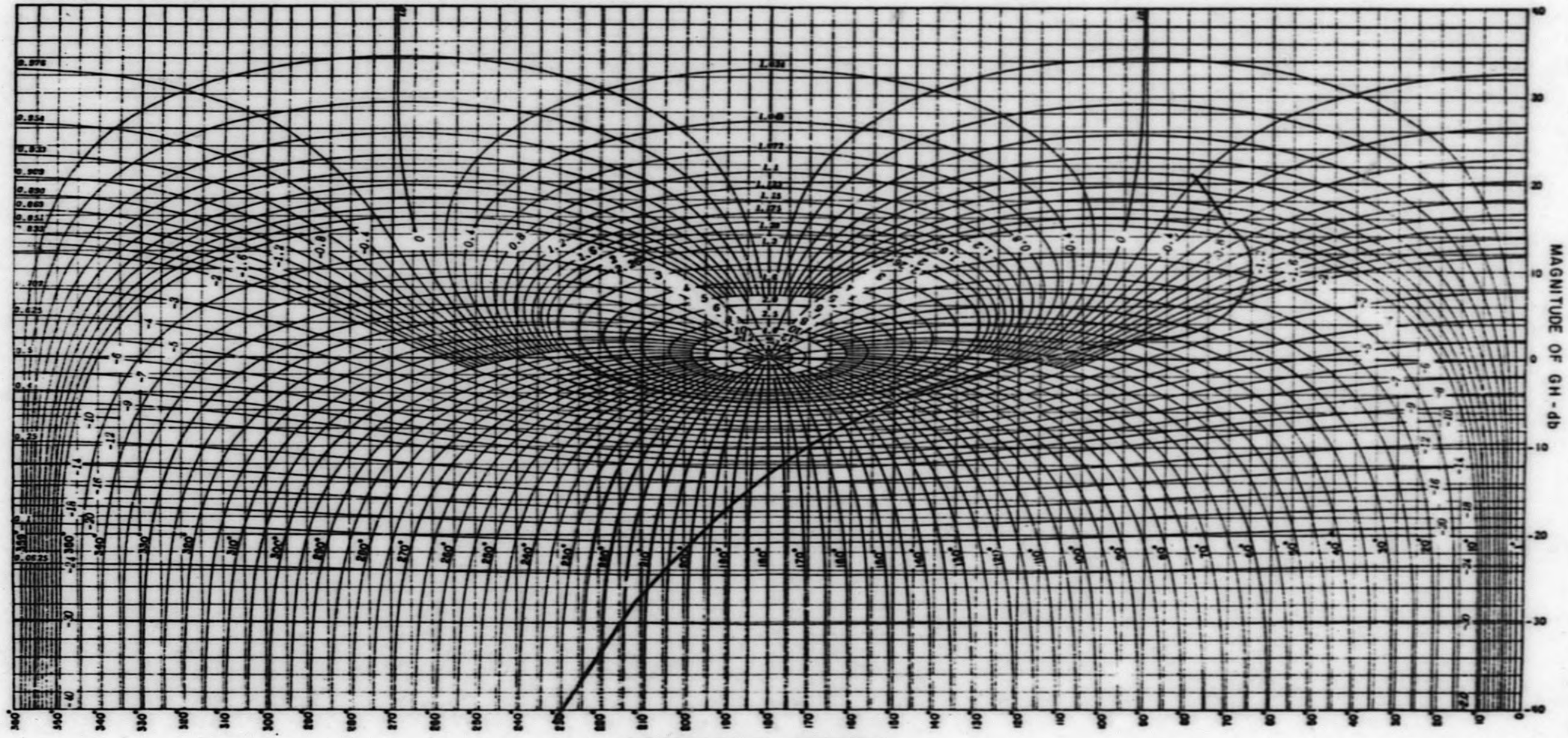

FIGURE 9

PLOT OF $\frac{GH}{1+GH}$ IN THE GH PLANE

FIGURE 10

FREQUENCY RESPONSE CHARACTERISTIC OF THE REACTOR-RECIRCULATION LOOP- $\frac{Q^{\Phi}}{\Delta K}$ (CLOSED LOOP) $\left(\frac{G}{1+GH}\right)$

RATED CONDITIONS
50 MW CORE
VOID WORTH — $ 4.50

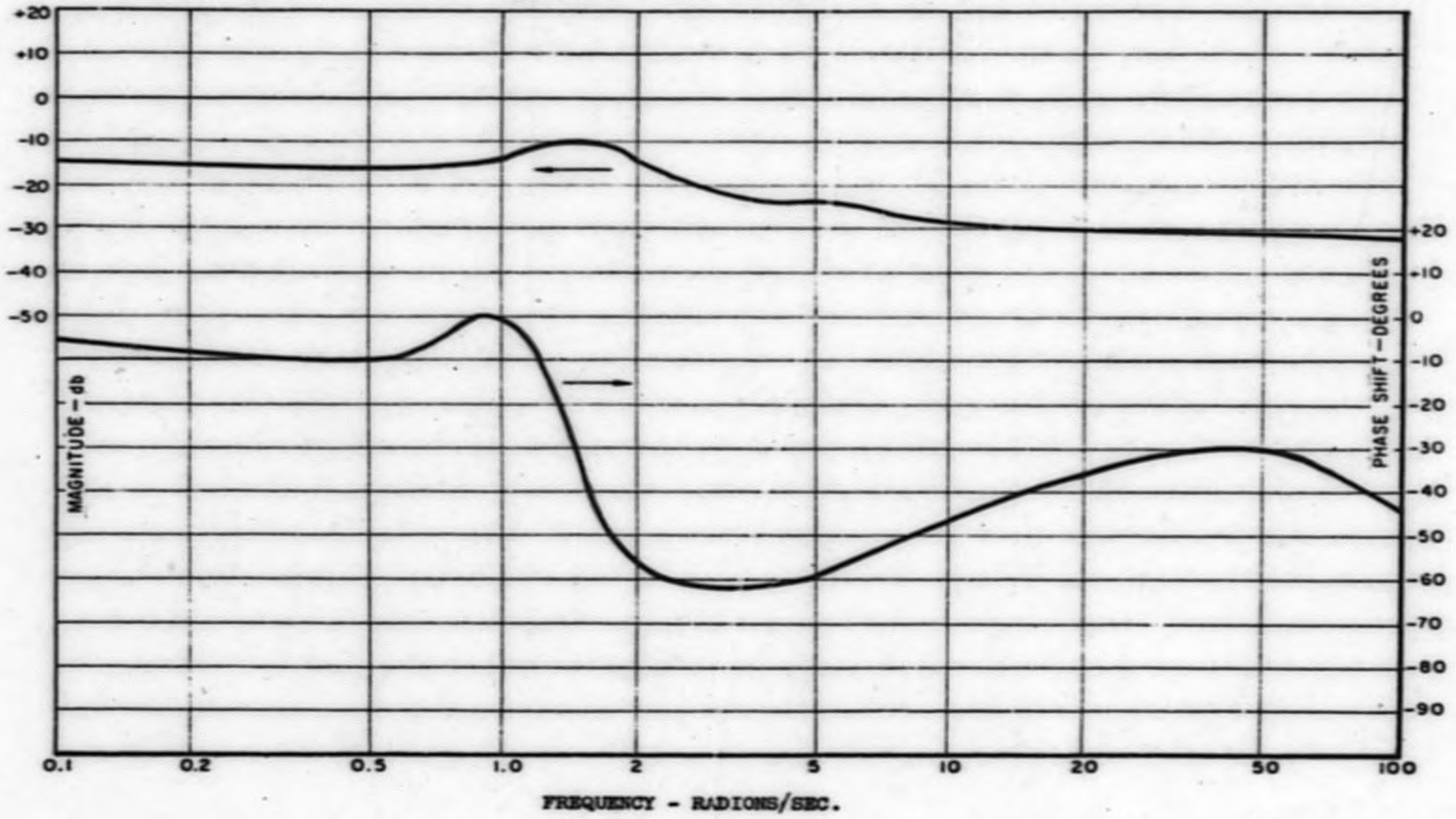

FIGURE II
FREQUENCY RESPONSE CHARACTERISTIC OF PRESSURE RATE,
PRESSURE VOIDS & PRESSURE REACTIVITY LOOP - $\Delta K_P / Q^{\#}(K)$

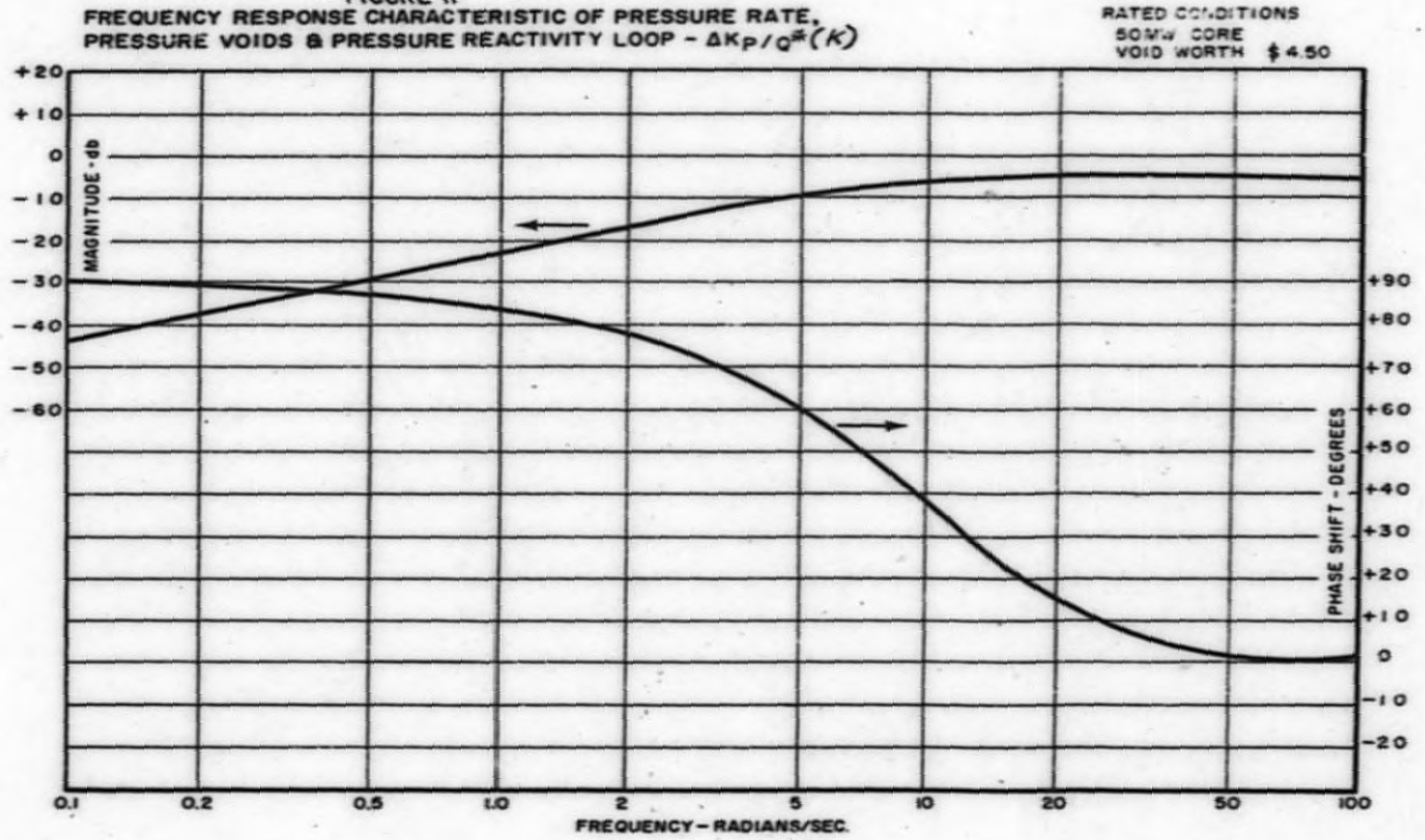

FIGURE 12
FREQUENCY RESPONSE CHARACTERISTIC OF REACTOR-RECIRCULATION LOOP & PRESSURE GENERATED REACTIVITY $\Delta K_{P}/\Delta K$ (OPEN LOOP) $\left(\frac{GK}{1+GH}\right)$

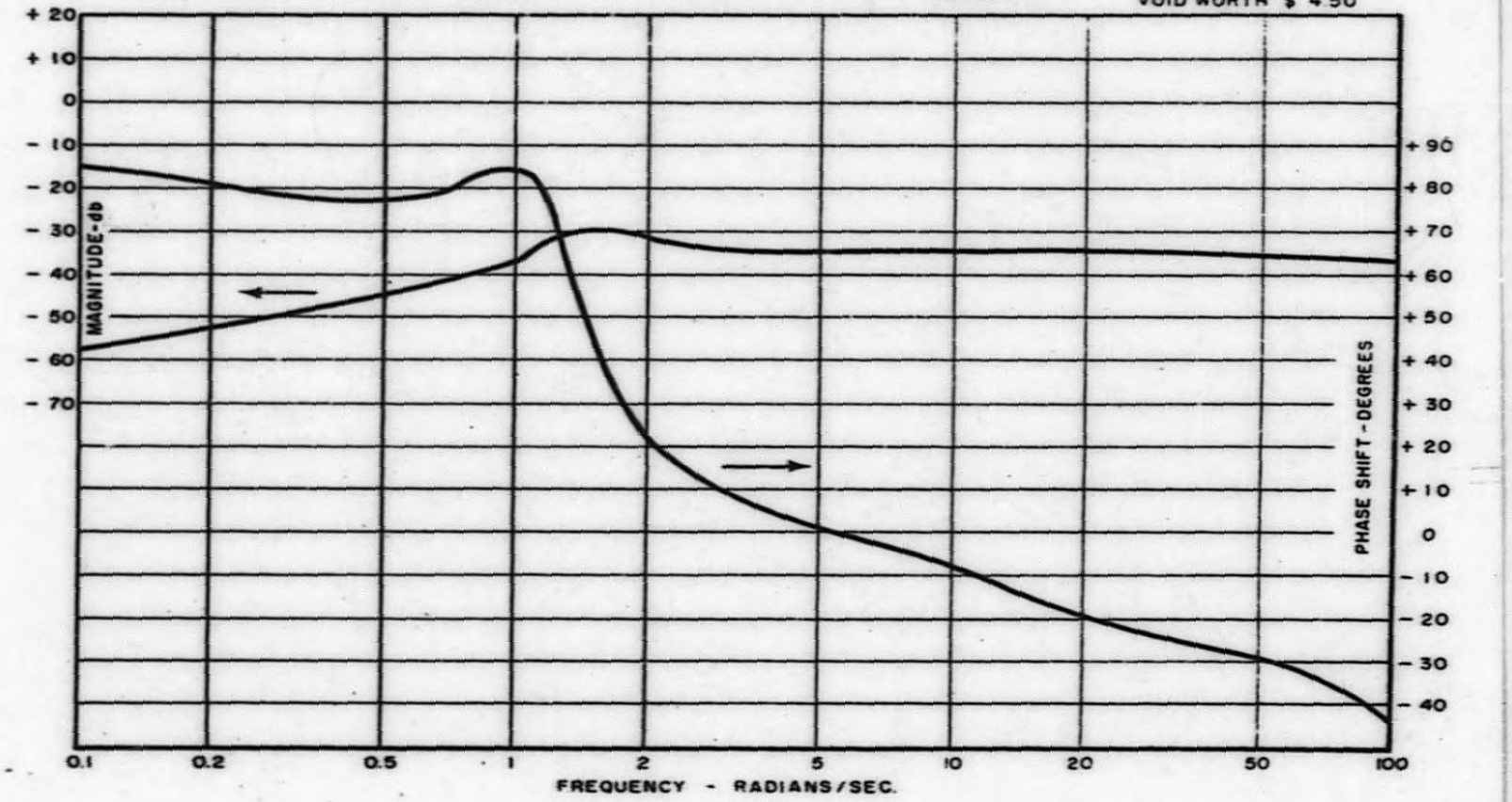

FIGURE 13
FREQUENCY RESPONSE CHARACTERISTIC OF THE
FLOW LOOP HYDRODYNAMICS - $\Delta K_Q/Q^*(H)$

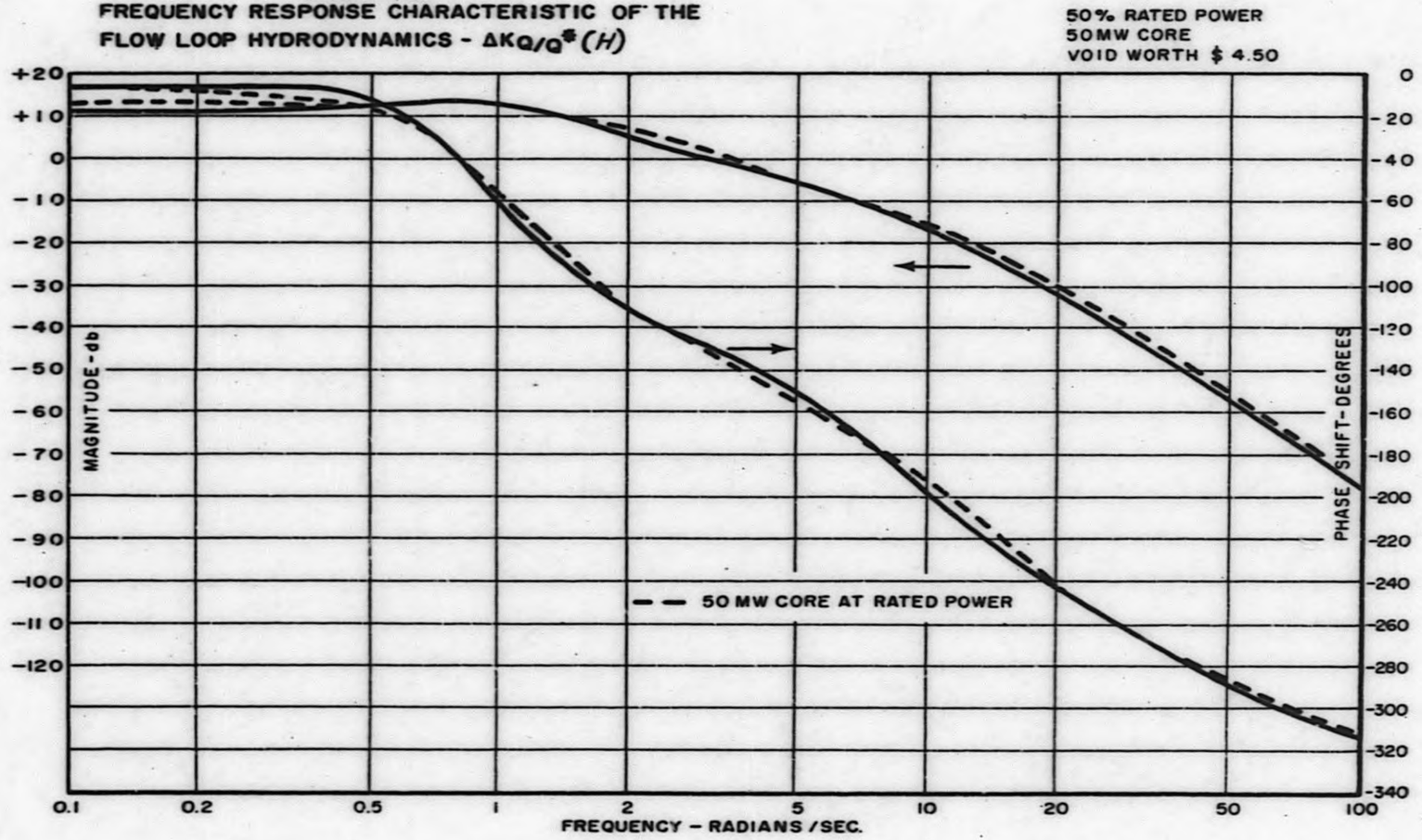

FIGURE 14
FREQUENCY RESPONSE CHARACTERISTIC OF THE
REACTOR-RECIRCULATION LOOP - $\Delta K_Q/\Delta K$ (OPEN LOOP) (GH)

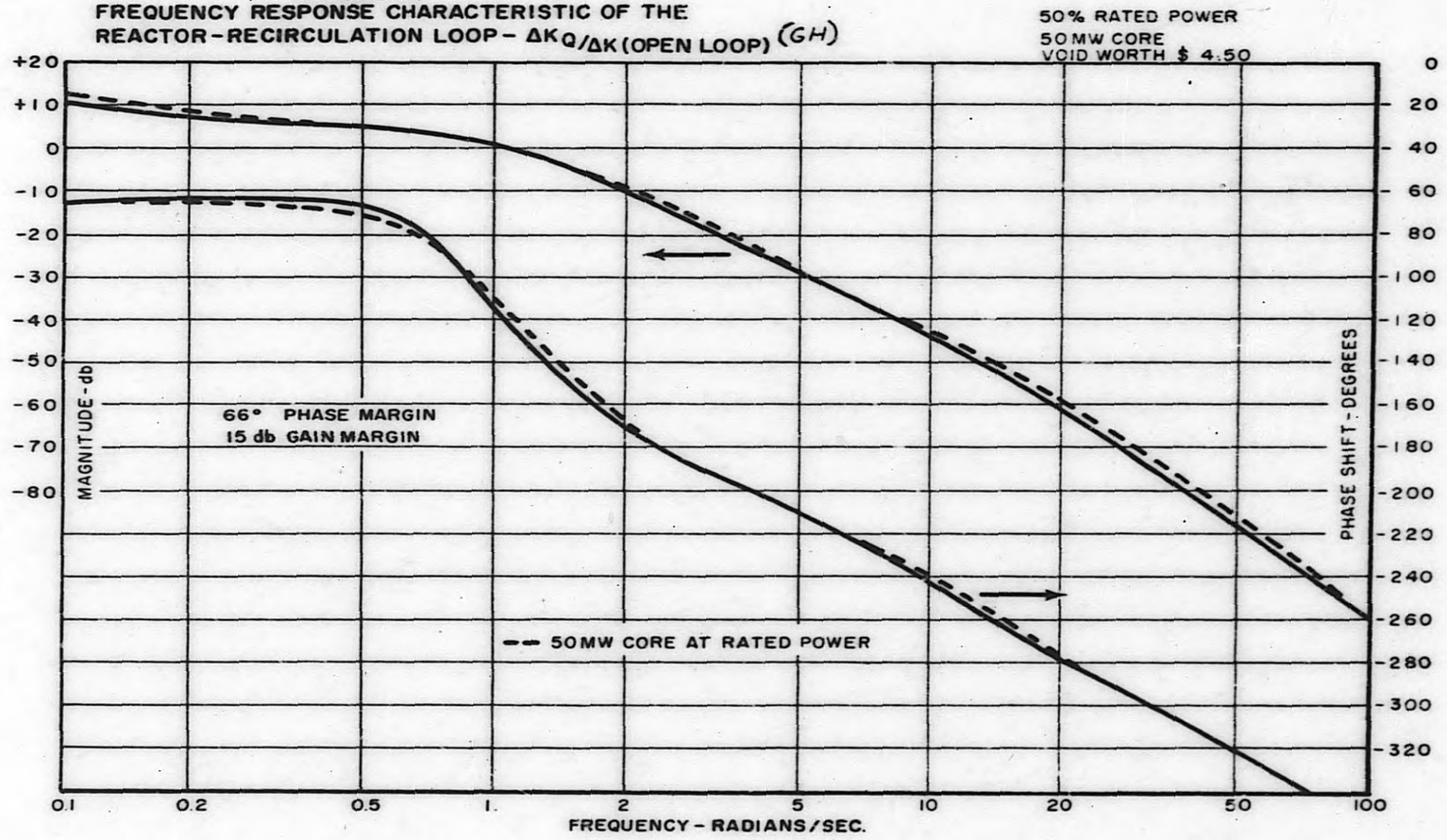

FIGURE 15
FREQUENCY RESPONSE CHARACTERISTIC OF THE
FLOW LOOP HYDRODYNAMICS - $\Delta K_{Q/Q}*(H)$

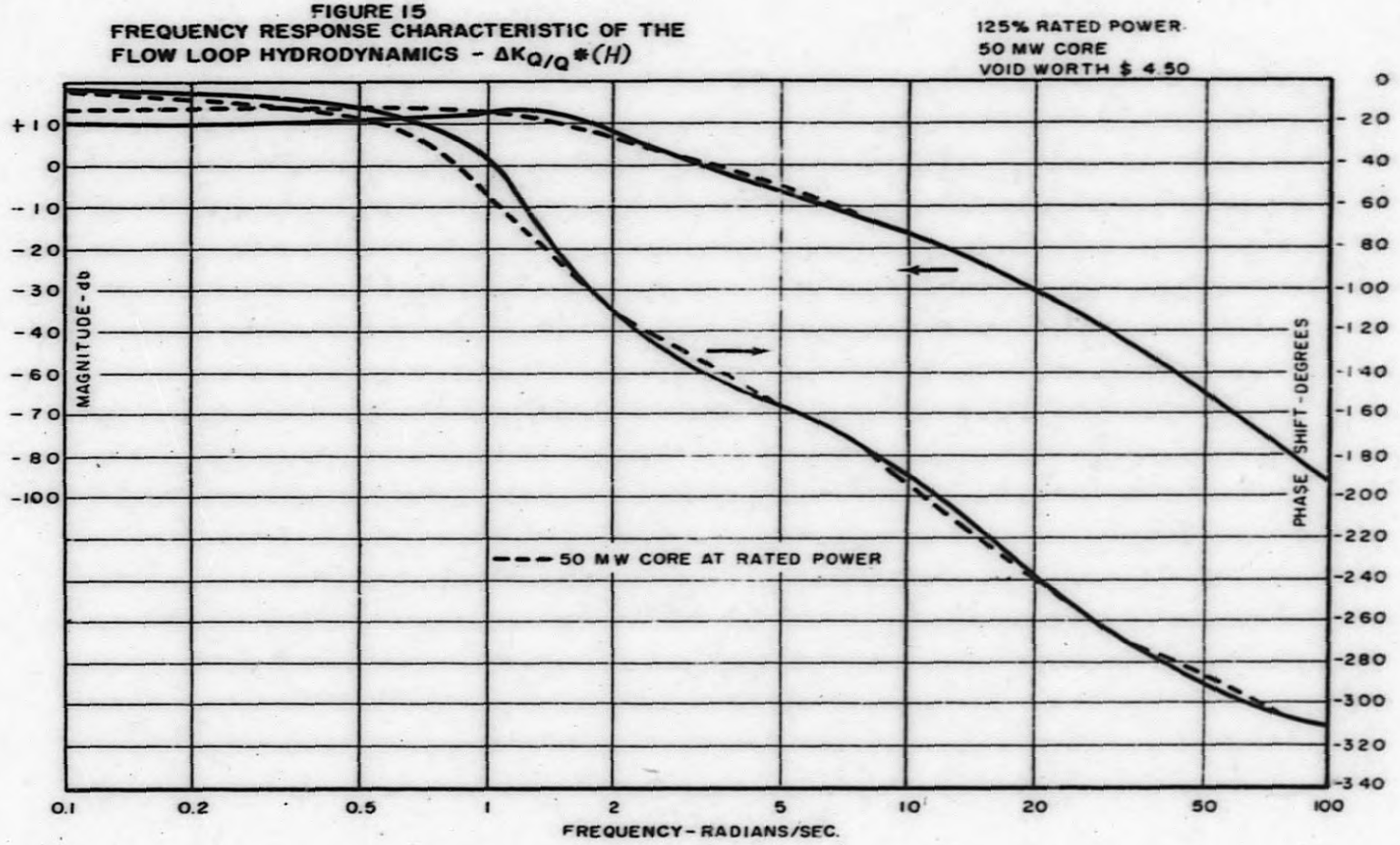

FIGURE 16
FREQUENCY RESPONSE CHARACTERISTIC OF THE
REACTOR-RECIRCULATION LOOP – $\Delta K_Q/\Delta K$ (OPEN LOOP) (GH)

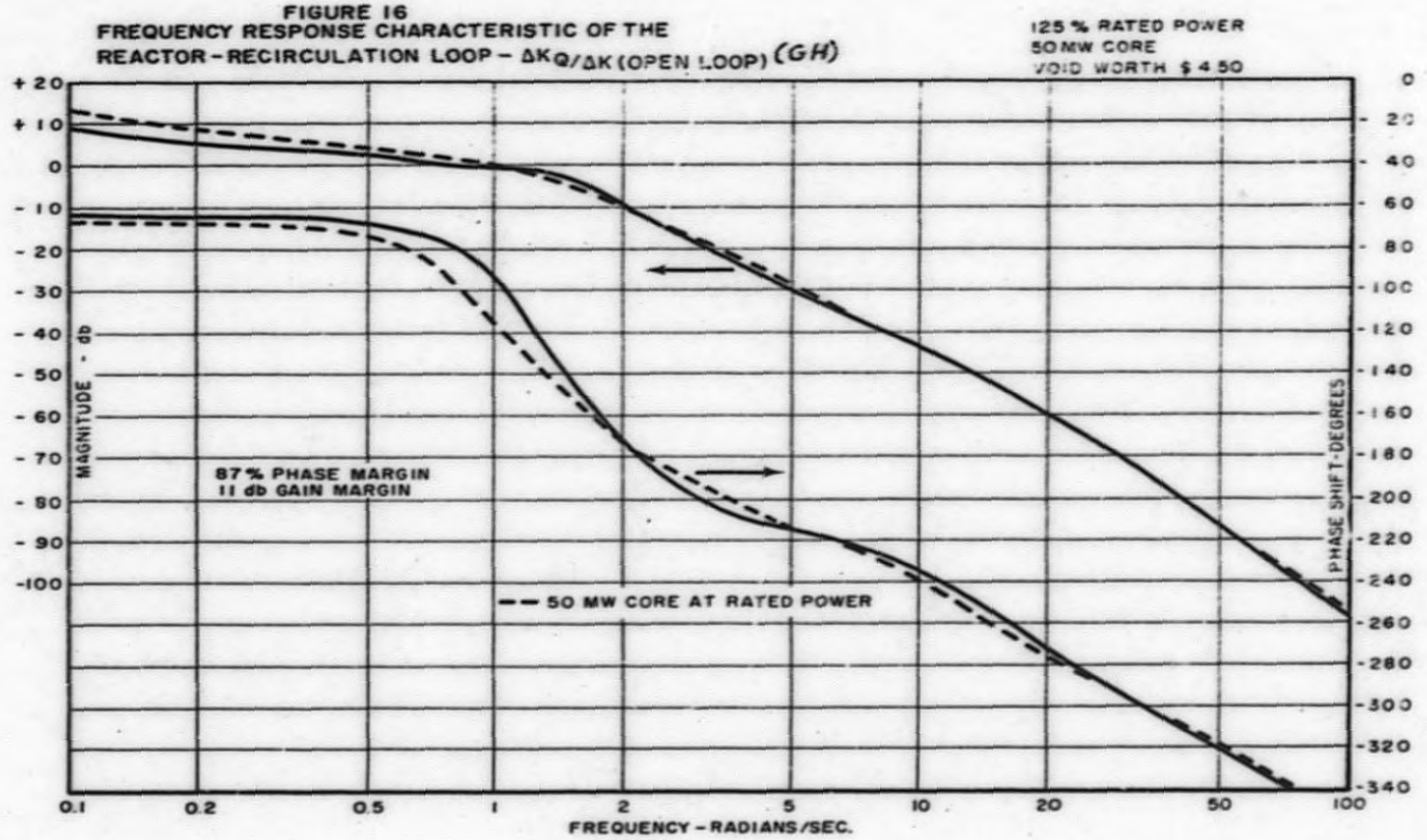

FIGURE-17
FREQUENCY RESPONSE CHARACTERISTIC OF THE FLOW LOOP HYDRODYNAMICS - $\Delta K_{Q/Q^*}(H)$

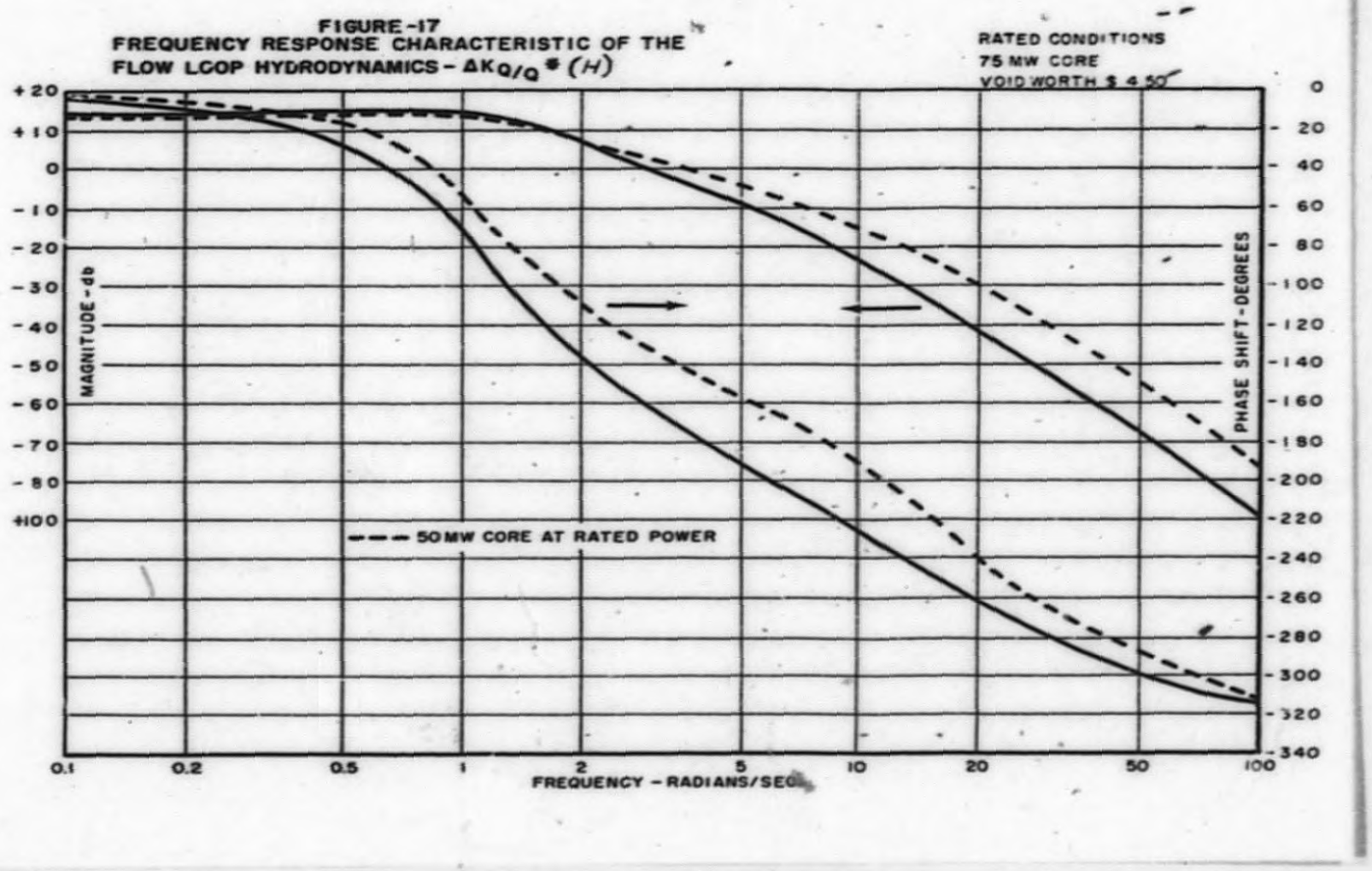

FIGURE 18
FREQUENCY RESPONSE CHARACTERISTIC OF THE
REACTOR-RECIRCULATION LOOP - $\Delta K_Q/\Delta K$ (OPEN LOOP) (GH)

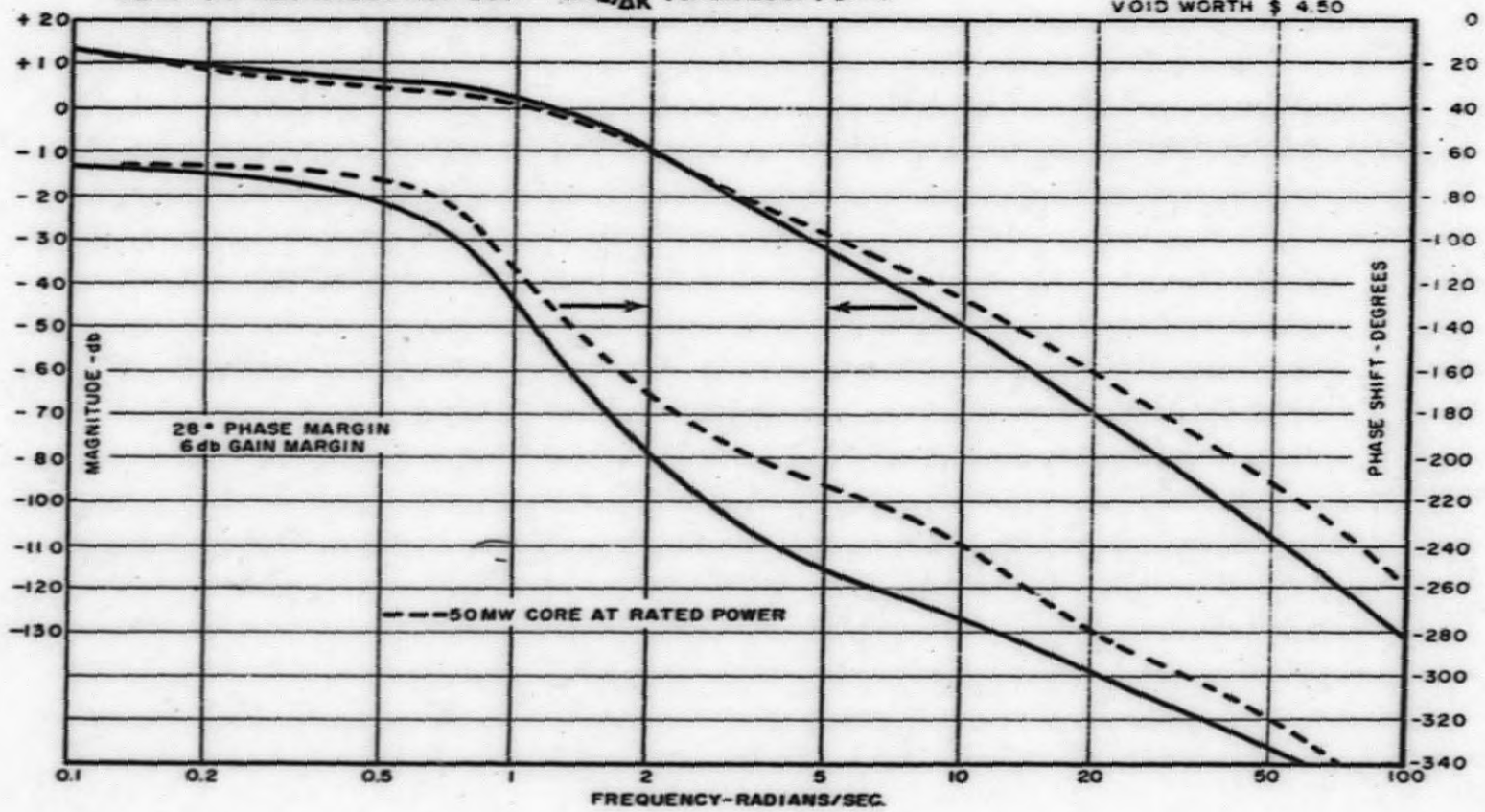

FIGURE 19
NOISE PERFORMANCE ANALYSIS

HOT CHANNEL OF THE 50MW CORE
AT RATED CONDITIONS
VOID WORTH - $ 4.50

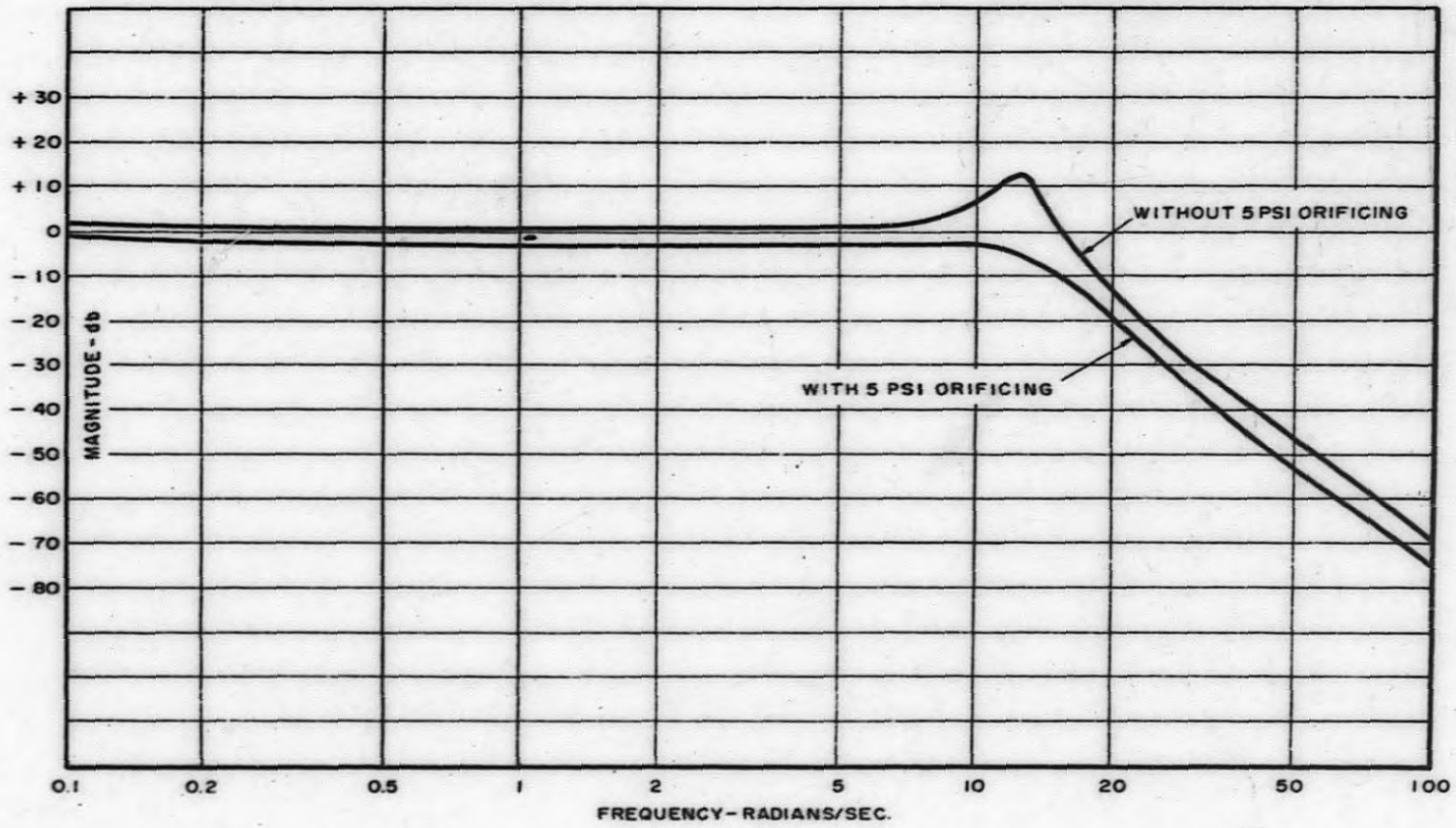

ACKNOWLEDGEMENTS

The authors wish to extend their appreciation and gratitude to Mr. E. S. Beckjord for his assistance during the course of this analysis and Drs. W. H. Cook and R. O. Niemi for their suggestions concerning the presentation of this report.

REFERENCES

[1] Case, J. M., "Neutron and Parallel Flow Channel Coupling Effects on the T-7 Flux Trap Reactor", GEAP-3508.

[2] Beckjord, E. S., and Harker, W. H., "The Steady-State Calculation of Vertical Two-Phase Flow", GEAP-3261.

[3] Beckjord, E. S., "The Stability of Two-Phase Loops and Response to Ship's Motion", GEAP-3493, Revision 1.

[4] Quinn, E. P., and Case, J. M., "Natural Circulation Loop Performance at 1000 psia Under Periodic Accelerations", GEAP-3397, Revision 1.

[5] Schultz, M. A., "Control of Nuclear Reactors and Power Plants", N. Y., McGraw-Hill, 1955.

[6] Pflasterer, G. R., and Romeo, R. J., "Personal Communication".

[7] Holland, L. K., "Heat Transfer from a Cylindrical Rod with Internal Heat Generation", GEAP-0805.

[8] Weil, J. W., et al, "Boiling Water Reactor Stability", General Electric Company Bulletin, GER-1468, page 19.

[9] Case, J. M., VBWR Flux Noise Predictions, unpublished report.

[10] Chestnut, H., and Mayer, R. W., "Servomechanisms and Regulating System Design", John Wiley and Sons, Inc., New York, 1948.

[11] Akcasu, Z., and Thie, J. A., "Methods of Investigating Noisy Power Reactors", ANL-6205.

APPENDIX A

THE HYDRODYNAMIC ANALYSIS

The transient two-phase flow model used in this study is based upon an analysis which was developed for the description of a single node natural circulation loop with point heat input.[3] This analysis can be described by a system of six (6) equations which are established upon the physical concepts of momentum interchange, conservation of energy and continuity of mass and not upon steam void versus quality correlations, or assumed ratios or differences between steam velocity and water velocity in the two-phase region. Five of the six equations are applied directly to a description of the flow behavior in the two-phase region of the loop and the remaining equation relates the pressure contribution of the downcomer or recirculation loop to that of the two-phase region.

It was necessary for the purposes of this stability analysis to further develop the hydrodynamic model so that:

A. It would accept forced circulation flow problems.

B. The rather involved mathematical solutions could be reduced to a linearized transfer function acceptable for a frequency-phase shift analysis (Bode' analysis).

C. Solutions could be readily obtained.

The following describes how the above objectives were achieved:

Modification of the Hydrodynamic Analysis for Forced Circulation

Figure 20 is a schematic diagram of the physical two-phase flow system conceived for this hydrodynamic model. The following five (5) transient equations were written for the two-phase flow region:

Momentum equation for water and steam:

$$\Pi + \frac{1}{L_B + L_R}\left[\left(1 - \frac{R}{2}\right)\frac{W^2 - V^2}{2}\right] + \frac{W}{2}^2 (\text{POLY } U)\left[\frac{L_R G_{WR} + K_R + L_B G_{WH}}{L_B + L_R}\right] \quad (24)$$
$$+ (1-R)_g + C(1-R)\frac{dW}{dt} = 0$$

WHERE: Poly $U = a_0 + a_1 R + a_2 R^2 + a_3 R^3 + \cdots + a_6 R^6$

Momentum equation for steam:

$$\Pi + G_{WS}\frac{(S-W)^2}{2}\left[1 - X + \frac{X}{\beta}\right] S(R) = 0 \quad (25)$$

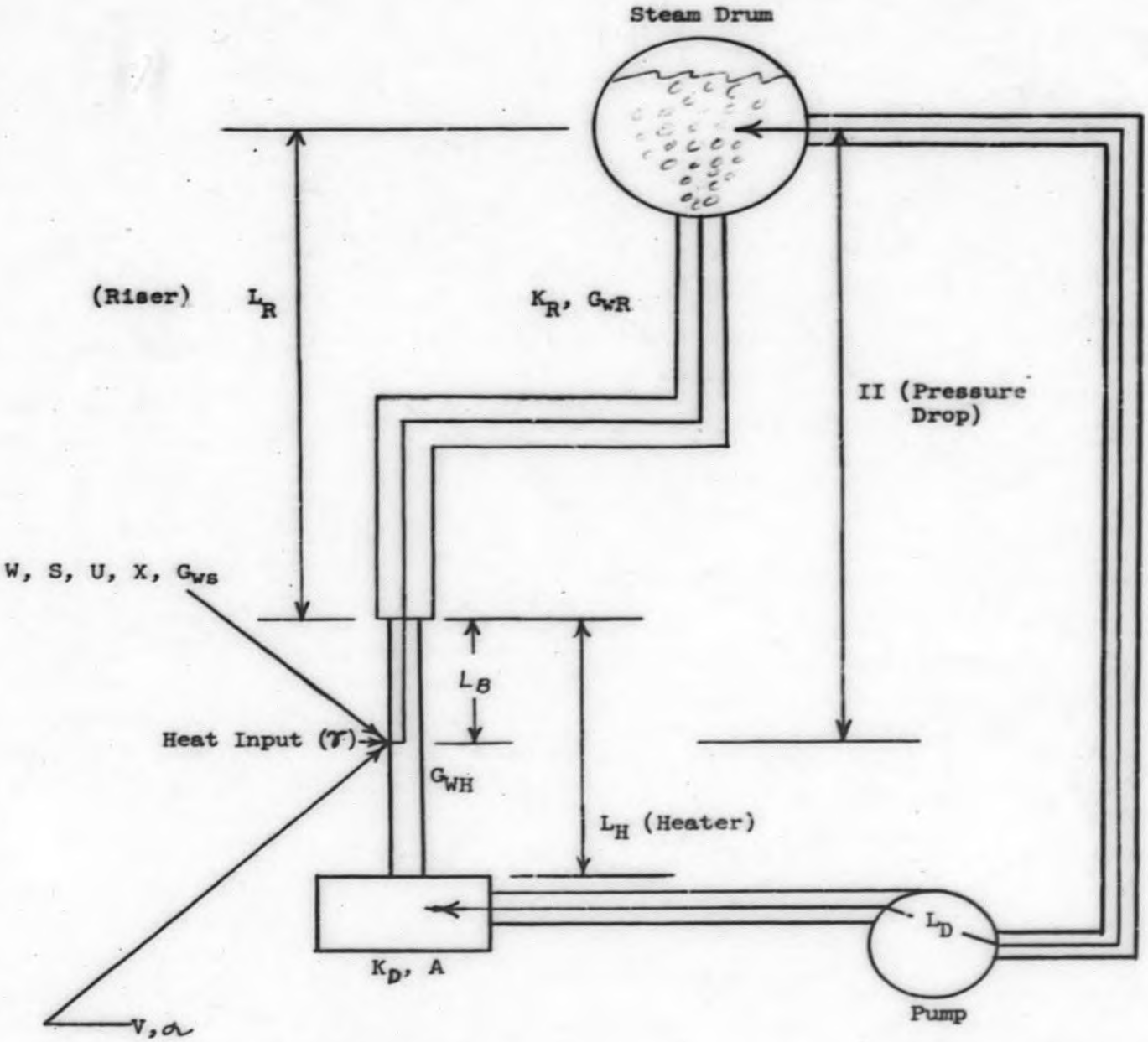

$$C = \frac{\text{Path length of riser}}{\text{Vertical length of riser}} \qquad D = \frac{\text{Flow area of riser}}{\text{Flow area of heater}}$$

Figure 20
Schematic Diagram of the Hydrodynamic Model

WHERE: $X = \frac{US}{\beta V}$ and $\delta(R) = \begin{cases} 1 : R < 0.5 \\ \frac{1-R}{R} : R \geq 0.5 \end{cases}$

Continuity of mass and energy equations across the boiling boundary.

$$R(S-W)+W = V(1+\alpha-\alpha\beta)+(\beta-1)Y \qquad (26)$$

$$(1-U)W = V(1+\alpha)-Y \qquad (27)$$

The transport equation of average voids versus boiling boundary voids:

$$R = \frac{1-e^{T_{T-P}S}}{T_{T-P}S}\,U \qquad (28)$$

WHERE: S = Complex Laplace Operator

$$T_{T-P} = \frac{L_R\,(C)(D)+L_B}{W}$$

$$L_B = L_H\left(1 - \frac{\Delta Y}{Y}\right)$$

Pressure drop across the two-phase flow region was related to the external recirculation loop flow by a single-phase momentum equation:

$$\Pi + g - \frac{V^2}{2}\left[\frac{L_D A + K_D + (L_H - L_B)G_{WH}}{L_B + L_R}\right] + \left[\frac{POLY\ P}{L_B+L_R}\right] - \left[\frac{L_D + L_H - L_B}{L_B + L_R}\right]\frac{dV}{dt} = 0 \qquad (29)$$

WHERE: Poly Pump = $b_0 + b_1V + b_2V^2 + \cdots b_6V^6$

It was the addition of the pump polynomial term in Equation 29 which made this heretofore natural circulation hydrodynamic analysis compatible with forced circulation problems.

Linearized Transient Analysis

Loop dynamics can be investigated for small disturbances by the transformation, linearization and normalization of the foregoing transient equations:

A. Transformation - conversion of the equation from the time to the frequency domain by Laplace transformation.

B. Linearization - the variables are expanded in a Taylor series about a steady-state solution and second order terms and cross products are ignored.

C. Normalization - the incremental variation in each parameter is divided by its steady-state value which reduces the incremental change to a fractional variation of steady-state conditions (per unit values).

Performance of the above mentioned operations upon the foregoing transient equations yields:

$$\frac{dW}{dt} = -\left[\frac{\Pi_o}{C(1-R_o)W_o}\right]\Pi^* + \left[\frac{R_o}{C(1-R_o)W_o}\left(\frac{W_o^2 - V_o^2}{4(L_R+L_B)} + g\right)\right]R^*$$

$$-\left[\frac{V}{C(1-R_o)W_o(L_B+L_R)^2}\left(-(L_B+L_R)(1-\frac{R_o}{2})V_o + (1-\frac{R_o}{2})(\frac{W_o^2-V_o^2}{2})\frac{L_H\alpha}{\gamma} - \frac{W_o^2}{2}(POLY\,U)\frac{L_H\alpha}{\gamma}\left(L_R(G_{WH}-G_{WR})-K_R\right)\right]V^*\right.$$

$$-\left[\frac{W_o}{C(1-R_o)(L_R+L_B)}\left((1-\frac{R_o}{2}) + (POLY\,U)(L_R G_{WR} + K_R + L_B G_{WH})\right)\right]W^*$$

(30)

$$+\left[\frac{L_H\alpha V_o}{\gamma_o C(L_B+L_R)^2(1-R_o)W_o}\left((1-\frac{R_o}{2})(\frac{W_o^2-V_o^2}{2}) - \frac{W_o^2}{2}(POLY\,U)(L_R(G_{WH}-G_{WR}-K_R)\right)\right]\gamma^*$$

$$\Pi^* = -\left[\frac{G_{WS}(1-x+\frac{x}{3})(S_o-W_o)^2\sigma(K)}{\Pi_o}\right](S-W)^* + \left[\frac{G_{WS}(1-x+\frac{x}{10})(S_o-W_o)^2}{2\Pi_o R_o}\right][\epsilon]R^* \quad (31)$$

WHERE: $\epsilon = \begin{cases} 0 : R \le 0.5 \\ 1 : R > 0.5 \end{cases}$

$$(S-W)^* = -R^* - \left[\frac{W_o}{(S_o-W_o)R_o}\right]W^* + \left[\frac{V_o(1+\lambda-\alpha\beta)}{(S_o-W_o)R_o}\right]V^* + \left[\frac{(\beta-1)\gamma_o}{(S_o-W_o)R_o}\right]\gamma^* \quad (32)$$

$$\frac{dU^*}{dt} = -\left[\frac{(1+\alpha)\,4V_o}{U_o L_B}\right]V^* + \left[\frac{4V_o}{U_o L_B}\right]\Gamma^* - \left[\frac{4W_o}{L_B}\right]U^* + \left[\frac{(1-U_o)4W_o}{U_o L_B}\right]W^* \qquad (33)$$

$$R^* = [DEL]\,U^*$$

WHERE:
$$[DEL] = \frac{1 - e^{-T_{T-P}S}}{T_{T-P}S} \qquad (34)$$

$$\frac{dV^*}{dt} = +\left[\frac{\Pi_o(L_B+L_R)}{(L_D+L_H-L_B)V_o}\right]\Pi^*$$
$$+\left[\left(\frac{L_H\alpha V_o^2}{(L_D+L_H-L_B)2\Gamma_o(L_B+L_R)}\left(G_{WH}(L_R+L_H)+L_D A+K_D\right)\right) - \left(\frac{(POLY\,P)L_H\alpha}{\Gamma_o(L_B+L_R)(L_D+L_H-L_B)}\right)\right]\Gamma^*$$
$$+\left[-V_o\left\{\left(\frac{V_o L_H\alpha G_{WH}}{2\Gamma_o(L_D+L_H-L_B)} + \frac{(L_D A+K_D+(L_H-L_D)G_{WH}}{(L_D+L_H-L_B)(L_B+L_R)}\left((L_B+L_R)+\frac{V_o L_H\alpha}{2\Gamma}\right)\right)\right\}\right.$$
$$\left.+\left\{\frac{(POLY\,P)\left(\frac{L_H\alpha}{\Gamma}\right)+(L_B+L_R)\,Z/V_o}{(L_D+L_H-L_B)(L_B+L_R)}\right\}\right]V^* \qquad (35)$$

WHERE:
1. subscript (o) denotes the steady-state value of the parameter.
2. superscript (*) denotes the variation of the parameter about the steady-state average: expressed in per unit values.

The steady-state solutions are found by setting the time derivatives in Equations (24) - (29) equal to zero and solving the resulting system of equations simultaneously.

It should be noted that Equation (33) does not follow directly from the linearization and normalization of algebraic Equation (27). It was here that cognizance was taken of the apparent deficiency in the point heat input assumption and an additional degree of freedom was added to the system in the form of a void equation time constant. This time constant was selected arbitrarily to be equivalent to 1/4 the void transit time across the boiling length of the heater section.

Justification for the existence of the additional time constant in the analysis

can be presented, however, it is immaterial for the Big Rock study since it was observed during the analysis that its presence had no noticeable effect whatsoever. The reason for this time constant's passive contribution to the analysis was that its frequency response was quite well beyond the frequencies of interest.

Equation (35) is the linearized and normalized external recirculation loop transient equation. It is this equation which takes into account the damping effect of external flow loop friction. The degree to which this friction damps the system depends upon how the two-phase flow loop is defined. The Z parameter in Equation (35) is an accommodation for varying the damping effect of the external flow loop.

It should be noted at this point that this hydrodynamic model was applied to the Consumers reactor in two different ways:

1. Loop hydrodynamics - the whole reactor core, two-phase risers, steam drum and recirculation loop were investigated for their combined dynamic response and feedback contribution to system stability.

2. Parallel flow channel hydrodynamics - a single hot channel within the reactor core was investigated for its performance in parallel with the rest of the core for expected operating flux noise predictions.

The loop hydrodynamic analysis above requires that full account must be taken of the pressure drop producing elements or friction in the downcomer. This is so, of course, because flow continuity must exist between the whole core and the recirculation loop. The parallel flow channel hydrodynamic analysis, however, assumes continuity of mass between the sum of each core flow channel and the external recirculation flow. That is, a flow variation which occurs in a single core channel must be balanced by either a re-distribution of flow between channels in the reactor core or a change in the total recirculation loop flow or the combined effect of both. An exact representation of this flow arrangement is quite difficult to accomplish because the large number of simultaneous equations in the resulting model make the analysis almost prohibitive. It was concluded, for the purposes of this study, to adopt a pessimistic view of the parallel flow channel mechanism. The flow in any single hot channel within the reactor core is very small compared with the total core flow. Therefore, its flow behavior is not damped by either the external recirculation loop flow or the balance of the core flow in the rest of the parallel channels. A parallel flow channel dynamic investigation based upon the foregoing assumption will produce predicted amplitudes which are higher than actual.

Solutions were obtained for both 1. loop hydrodynamics and 2. parallel flow channel hydrodynamics by the use of the above described analytical model. Briefly, the procedure was the following:

1. Loop hydrodynamics - the input information for the model was selected to agree with the geometry and thermodynamics of the whole reactor core, two-phase risers, steam drum and recirculation loop. The Z parameter in transient Equation (35) was adjusted to reflect the slope of the

external loop pressure drop versus flow curve at the steady-state flow condition. This slope was taken from a single-phase V^2 loss curve passed through the steady-state operating condition from the shut-off head of the pump. Z = 2 (Poly Pump - shut-off head of the pump). This was equivalent to saying that the two-phase loop damping caused by the external recirculation loop followed a single phase V^2 loss curve.

2. Parallel flow channel hydrodynamics - the input information for the model was selected to agree with the geometry and thermodynamics of the hot fuel channel in the reactor core. The Z parameter in transient Equation (35) was set equal to zero. This was equivalent to saying that the hot channel received no damping from its parallel channels or the recirculation loop (a conservative analysis).

The linearized and normalized transient Equations (30) - (35) can be rewritten in the following coefficient form:

$$II^* = 2\,(S - W)^* + a\,(R)^* \tag{36}$$

$$(S-W)^* = -(R)^* + b(W)^* + c(V)^* + d(\tau)^* \tag{37}$$

$$\frac{dv^*}{dt} = e(R)^* + f(II)^* + g(\tau)^* + h(V)^* + i(W)^* \tag{38}$$

$$\frac{dv^*}{dt} = j(II) + k(\tau)^* + l(V)^* \tag{39}$$

$$\frac{du^*}{dt} = m(w)^* + n(v)^* + o(\tau)^* + p\,(u)^* \tag{40}$$

$$R^* = (DEL)\,(U)^* \tag{41}$$

WHERE: Coefficients a-p are determined by the arithmetic evaluation of Equations (30) - (35).

The above system of equations can be solved simultaneously for the relationship between boiling boundary voids and heat input (u^*/τ^*). Performance of this mathematical manipulation yields:

$$\frac{U^*}{\gamma^*} = \frac{C_1 (S)^2 + C_2 (S) + C_3}{(S)^3 + K_1 (S)^2 + K_2(S) + K_3(DEL) (S) + K_4 + K_5 (DEL)} \qquad (42)$$

WHERE:

$C_1 = +0$

$C_2 = +2j \left[dn - co\right] + 2f \left[dm - bo\right] + kn - gm - o \left[1+1\right]$

$C_3 = +\left[2 fd + g\right] \left[(2jb) n - (2 jc + 1) m\right]$
$+\left[2 fb + i\right] \left[(2jc + 1) o - (2jd + k) n\right]$
$+\left[2 fc + h\right] \left[(2jd + k) m - (2jb) o\right]$

$K_1 = - \left[i + l + p + 2 (fb + jc)\right]$

$K_2 = (i + 2fb) (l + p) + lp + 2j (cp + ic - hb)$

$K_3 = - m \left[e + f (a - 2)\right] - jn (a - 2)$

$K_4 = - p \left[l (i + 2 fb) + 2j (ic - hb)\right]$

$K_5 = \left[e + f (a - 2)\right] \left[ml + 2j (mc - nb)\right] - j (a-2) \left[m (h + 2 fc) - n (i + 2fb)\right]$

Solving for the roots of Equation (42)

$$\frac{U^*_{a,h}}{\gamma^*} = \frac{GAIN\,1\left[1 + \tau_1(S)\right]\left[1 + \tau_2(S)\right]}{\left[1 + 2\xi \tau_3(S) + \tau_3^2(S)^2\right]\left[1 + \tau_4(S)\right]} = \frac{U^*_{a,h}}{Q^*} \qquad (43)$$

Equation (43) constitutes the form of the loop hydrodynamic transfer function used in this stability analysis.

The transfer function used for the parallel flow channel hydrodynamics was boiling boundary voids from subcooling (U^*/α^*). The presence of subcooling in this transfer function arises from the postulation that flux noise in a reactor is a consequence of minute temperature variations in the core inlet water. This transfer function, as a first order approximation, can be resolved from Equation (43) by a simple gain relationship. From the energy equation across the boiling boundary

$$\gamma - \alpha V = \frac{\mu S}{\beta} \qquad (44)$$

Solving for the relative influence of heat (τ) with respect to subcooling (α) for a constant steaming rate:

$$\alpha^* = -\tau^* \left[\frac{\tau_o}{V_o \alpha_o}\right] \qquad \text{(per unit values)} \qquad (45)$$

Equation (45) merely states that the effect of a subcooling change (α^*) is $-\frac{V_o \alpha_o}{\tau_o}$ as great as the same percentage change in heat (τ^*). Therefore, the U^*/α^* transfer function can be defined:

$$\frac{U^*_{noise}}{\alpha^*} = \text{EQUATION (43)}\left[-\frac{V_o \alpha_o}{\tau_o}\right] \qquad (46)$$

Analytical Flow Model Solution

The objective of the analytical flow model as it was used in this report was to obtain from basic design geometry and thermodynamics the loop hydrodynamics transfer function and the parallel flow channel hydrodynamic transfer function. (Eqs. 43 and 46). This objective was accomplished by using Equations 24 through 46 in the following three basic steps:

1. The steady-state solution for the nominal operating condition of the two-phase flow loop. This was a simultaneous solution of Equations 24-29 after the time derivatives were set to zero.

2. The solution of the linearized and normalized transient equations. This was just merely the arithmetical solution of Equations 30-35 using the steady-state solutions found in (1) above.

3. The solution of the transfer functions (Eqs. 43 and 46) using Equation 42 and the transient equation coefficients found in (2) above.

Solution of the analytical flow model was accomplished by the combined effort of digital computer solution and hand calculation. The first two steps in the flow model solution (1 and 2 above) were accomplished by the use of a digital computer code. The transfer functions (step 3 above) were obtained by hand calculations.

It should be mentioned that a validity check was made on the resolution of the transfer function from Equations 36-41. This was achieved by first obtaining an analogue solution for the frequency response of Equations 36-41 and then comparing this result with a Bode analysis of the transfer function. The two solutions were found to be identical.

Digital Computer Code Development

The ultimate digital computer code utilized for this analysis, 5-VLOP, was a modification of an existing natural circulation hydrodynamics analysis code, 3-VLOP. The analysis was modified to include the effects of forced circulation. The polynomial term which accounts for pumping effects in the total loop pressure drop Equation 29 reflects this change. The new code was programmed to solve this revised system of equations. The details of this code need not be presented here since it is essentially only the implementation of the solution of the system of equations described in this Appendix A.

The code accepts as input the thermodynamics and geometrical parameters which define the reactor system and are summarized for the Big Rock Point Reactor in Appendix C. The code then develops the appropriate coefficients for the transient Equations 36 through 41 and provides the initial steady state values of the variables V, W, S, II, U, L_B, and X for which the coefficients are applicable. The code does not develop the transfer function coefficients of Equations 43 and 46, this being done by hand for all cases considered in the study being reported.

APPENDIX B

CORE VOIDS

In this stability analysis all of the reactivity feedback with the exception of the Doppler influence is brought about by a change in the average steam void content within the reactor core. The average core void content is related, in turn, to two separate influences:

A. The contribution of heat and subcooling changes.

B. The contribution of pressure change.

The following describes how average core voids were related to the above two influences.

Heat and Subcooling Voids

Voids resulting from heat and subcooling changes are described at the boiling boundary of the fuel element by the $U^*_{Q,h}/\tau^*$ transfer function. (See Appendix A.) Average core voids owing to this influence can be described:

$$\bar{U} = \frac{1}{L}\int_0^L U(L,t)\,dL \tag{47}$$

and from continuity of the water in the two-phase flow region:

$$\frac{\partial}{\partial L}(1-U)A_{ff}\rho_w W + \frac{\partial}{\partial t}(1-U)A_{ff}\rho_w = 0 = U(L,t) \tag{48}$$

Assuming A_{ff},ρ_w and w constant with L and A_{ff},ρ_w constant with τ, Equation (48) reduces to:

$$W\frac{\partial U}{\partial L} + \frac{\partial U}{\partial t} = 0 = U(L,t) \tag{49}$$

from which a solution for U (L, τ) in delayed unit function form is obtained.

$$U(L,t) = U\left(t - \frac{L}{W}\right) \tag{50}$$

Substituting Equation (50) into Equation (47):

$$\overline{U} = \frac{1}{L}\int_{o}^{L} U(t - \frac{L}{W})\, dL \qquad (51)$$

and by change of variables:

$$\overline{U} = \frac{1}{L}\int_{t}^{\theta} U(\theta)(-W)\, d\theta \qquad (52)$$

WHERE: $\theta = t - L/W$

$$\overline{U} = +\frac{W}{L}\int_{t-L/W}^{t} U(\theta)\, d\theta$$

$$= \frac{W}{L}\left[\int_{o}^{t} U(\theta)\, d\theta - \int_{o}^{t-L/W} U(\theta)\, d\theta\right] \qquad (53)$$

Taking the Laplace transform of Equation (53):

$$\overline{U} = \frac{1 - e^{-T_c S}}{T_c S}\, U(S) \qquad (54)$$

WHERE: $T_c = LB/W$

From Equation (54) the desired transfer function can be obtained in per unit values:

$$\frac{\overline{U}}{U^*}^{*} = \frac{1 - e^{-T_c S}}{T_c S} = [DEL] \qquad (55)$$

The (DEL) operator of Equation (55) can be described with sufficient accuracy

for this analysis by a second order diagonal Padé approximation:

$$\frac{\overline{U_{ah}}^{*}}{U_{ah}^{*}} = \frac{1 - e^{-T_c S}}{T_c S} \approx \frac{1}{1 + \frac{T_c S}{2} + \frac{T_c^2 S^2}{12}} \qquad (56)$$

Pressure Voids

The effect of pressure variation upon the average core voids is almost exactly the opposite of the effect of heat and subcooling variation. A heat or subcooling variation causes the voids at the boiling boundary to change. Its influence upon the average core void can be described with time by an integral of this unit impulse as it sweeps up the core. A pressure variation, however, induces a flashing or collapse of the entire void content in the two-phase region. Its effect upon average core void is instantaneous and can be described with time by the initial flashing or collapse minus the integral of this unit impulse as it sweeps out of the core. The integral of this unit impulse or transient function is the (DEL) operator of Equation (55).

Further simplifing the (DEL) approximation of Equation (56):

$$\text{DEL} = \frac{1 - e^{-T_c S}}{T_c S} \approx \frac{1}{1 + \frac{T_c S}{2} + \frac{T_c^2 S^2}{12}} \approx \frac{1}{\left(1 + \frac{T_c S}{4}\right)^2} \qquad (57)$$

The transfer function of average core voids attributed to pressure ($\overline{U}^{*}p$) from voids induced by flashing or collapse ($U^{*}p$) can be described using Equation (57):

$$\frac{\overline{U_p}^{*}}{U_p^{*}} = \left[1 - (DEL)\right] \approx \left[1 - \frac{1}{\left(1 + \frac{T_c S}{4}\right)^2}\right] \qquad (58)$$

$$= \left[\frac{\frac{T_c S}{2}\left(1 + \frac{T_c S}{8}\right)}{\left(1 + \frac{T_c S}{4}\right)^2}\right]$$

APPENDIX C

REACTOR DATA SHEET FOR FIRST STABILITY ANALYSIS

	50 MWe Core	75 MWe Core
General Plant Data		
Gross MWe	50	75
Thermal MW	157.3	232.6
Core Exit Steam Flow, lbs/hr	568,700	930,400
Inlet Subcooling, Equiv., Btu/hr	15.0	23.6
Core Flow Rate, Total, lbs/hr	11.6×10^6	11.7×10^6
Feedwater Temp., °F	346.0	379.6
Pressure, psia	1050	1500
Core Description		
Configuration	K Lattice	K Lattice
No. of Assemblies	56	84
No. of Control Rods	24	32
Fuel Material	UO_2	UO_2
Clad Material	304 Stn. Stl.	304 Stn. Stl.
Moderator/Fuel Ratio, (Area)	2.7	2.7
Effective Active Fuel Length	70	70
Equiv. Core Diameter	62.5	76.5
Steam Volume Fraction:		
Avg. Quality in Channel Exit, %	5.5	9.1
Overall Average Moderator Voids	0.16	0.20
Max. Quality in Channel Exit, %	14.3	19.5
Max. at Channel Exit, Voids	0.65	0.65
Avg. Quality Entering Drum, %	5.2	8.2

	50 MWe Core	75 MWe Core
Design Hot-Spot Factor		
Overall	4.18	3.22
Avg. Fuel Ctr. Temperature, °F	1520	1550
Peak Fuel Temperature, °F	4,580	3,660
Peak Heat Flux, Btu/hr ft^2	463,000	352,000
Burnout Margin	1.5	1.5
Fuel		
No. of Fuel Rods/Assembly:		
Std. UO_2 Rods	131	131
Special Corner Rods	12	12
Diameter of Fuel Rods: (including jackets)		
Std. UO_2 Rods	0.388	0.388
Special Corner Rods	0.338	0.338
Fuel Rod Pitch	0.533	0.533
No. of Segments/Rod	1	1
Approx. Pellet Density, gr./cc (95% compaction)	10.4	10.4
Fuel Pellet Diameter:		
Std. UO_2 Rods	0.345	0.345
Special Corner Rods	0.297	0.297
Clad Thickness:		
Std. UO_2 Rods	0.019 ± 0.001	0.019 ± 0.001
Special Corner Rods	0.018 ± 0.001	0.018 ± 0.001
Heat Transfer Area, ft^2	4,690	7,035
No. of Channels	56	84
Channel Wall Thickness (Zr-2)	0.100	0.100
Inside Dimensions of Channels, in.	6.512 sq.	6.512 sq.

NOMENCLATURE

A	Single-phase friction factor of water against the wall in the recirculation portion of the flow loop -- ft^{-1}
A_{ff}	Flow area of the heater -- ft^2
B	Total fraction of delayed neutrons -- dimensionless
Bi	Fraction of the delayed neutrons of the i^{th} group -- dimensionless
C	Ratio of path length of the steam risers to the vertical length of the steam risers -- dimensionless
D	Ratio of the flow area of the risers to the flow area of the core -- dimensionless
G_{WH}	Single-phase friction factor of water against the wall in the heater -- ft^{-1}
G_{WR}	Single-phase friction factor of water against the wall in the riser -- ft^{-1}
G_{WS}	Friction factor of steam against water in the two-phase flow region -- ft^{-1}
g	Acceleration of gravity -- ft/sec^2
h_f	Enthalpy of saturated water -- Btu/lbm
h_g	Enthalpy of saturated steam -- Btu/lbm
h_{fg}	Enthalpy change due to vaporization ($h_g - h_f$) -- Btu/lbm

h_{fw}	Enthalpy of feedwater -- Btu/lbm
h_R	Enthalpy of recirculation water -- Btu/lbm
h_s	Subcooling enthalpy ($h_f - h_R$) -- Btu/lbm
J	Mechanical equivalent of heat -- 778 ft-lb_f/Btu
K_D	Single-phase head loss coefficient of the recirculation loop -- dimensionless
K_R	Single-phase head loss coefficient of the risers -- dimensionless
ℓ^*	Average neutron lifetime -- sec.
L	Length -- ft
L_B	Boiling length of heater -- ft
L_D	Path length of the recirculation loop -- ft
L_H	Heater length -- ft
L_R	Vertical length of the risers -- ft
Mf	Saturated water in the core -- lbm
Mg	Saturated steam in the core -- lbm
N	Power - neutron density -- neutrons/cm
P	Pressure -- psia
$\dot{P}$	Time rate of pressure change -- psi/sec

Q	Heat -- Btu/sec
R	Average voids in the two-phase flow region -- dimensionless
S	Steam velocity in the two-phase flow region -- ft/sec
(s)	Complex Laplace operator
t	Time variable -- sec
t_i	Time constant of i^{th} delay group -- sec
$\overline{t}$	Average time constant of the six delay groups -- sec
$\overline{T}$	Average fuel rod temperature -- ^{o}F
Tc	Core transit time -- sec
T_{T-P}	Two-phase region transit time -- sec
U	Voids at the boiling boundary of the heater -- dimensionless
U_{Qh}	Voids at the boiling boundary due to heat and subcooling -- dimensionless
U_{noise}	Voids at the boiling boundary due to noise excitation -- dimensionless
U_p	Voids due to pressure -- dimensionless
$\overline{U}_{Qh}$	Average voids within the core due to heat and subcooling -- dimensionless
$\overline{U}_p$	Average voids within the core due to pressure -- dimensionless

V	Water velocity in the single-phase region of the heater -- ft/sec
v	Volume of saturated steam and water in reactor vessel -- ft^3
v_c	Volume of saturated steam and water in reactor core -- ft^3
v_f	Specific volume of saturated water -- ft^3/lbm
v_g	Specific volume of saturated steam -- ft^3/lbm
v_{fg}	Specific vclume change due to vaporization (vg - vf) -- ft^3/lbm
W	Water velocity in the two-phase flow region -- ft/sec
W_f	Saturated water in the reactor vessel -- lbm
W_g	Saturated steam in the reactor vessel -- lbm
w_{FW}	Weight rate of feedwater flow -- lbm/sec
w_g	Weight rate of steam flow -- lbm/sec
W_R	Weight rate of recirculation flow lbm/sec
X	Steam quality -- %
ΔK	Excess multiplication factor or delta k -- dollars
ΔK_D	Delta k due to Doppler -- dollars
ΔK_h	Delta k due to subcooling -- dollars
ΔK_{noise}	Delta k due to noise -- dollars

ΔK_p	Delta k due to pressure -- dollars
ΔK_Q	Delta k due to heat -- dollars
ΔK_{rod}	Delta k due to control rods -- dollars
α	h_s/h_{fg} -- dimensionless
β	v_g/v_f -- dimensionless
γ	$\frac{Q\, V_f}{h_{fg}\, A_{ff}}$ -- ft/sec
ξ	Damping ratio -- dimensionless
θ	Auxiliary time variable -- sec
II	$\frac{\Delta P\, V_f\, 1449}{\Delta L}$ -- ft/sec^2
τ	Time constant -- sec
ω	Frequency -- rad/sec